

**Lu-Hf and Sm-Nd Systematics of Apollo 17 Sample  
78236: Ages, Evolution and Investigations into the  
Neutron Fluence Correction on the Lu-Hf System**

---

A Thesis

Presented to

the Faculty of the Department of Earth and Atmospheric Sciences

University of Houston

---

In Partial Fulfillment

of the Requirements for the Degree

Master of Science

---

By

Samuel Tyer Simmons

December 2012

**Lu-Hf and Sm-Nd Systematics of Apollo 17 Sample 78236: Ages,  
Evolution and Investigations into the Neutron Fluence Correction on  
the Lu-Hf System**

---

**Samuel Tyer Simmons**

**Approved:**

---

**Dr. Thomas J. Lapen, Advisor**

---

**Dr. Alan D. Brandon**

---

**Dr. Rasmus Andreasen**

---

**Dr. David S. Draper**

---

**Dr. Mark A. Smith, Dean, College of Natural Sciences and Mathematics**

## **Acknowledgements**

I would first like to thank my advisor Dr. Tom Lapen for contributing all his knowledge and so much of his time to my research and for allowing me to work on such an amazing project. I would like to thank my amazing committee: Dr. Rasmus Andreasen, Dr. Alan Brandon, and Dr. David Draper for answering all of my questions and for being so supportive during this entire process. I would like to thank Dr. Minako Richter for help in the clean lab and Dr. Yongjun Gao for help with the trace element work. I would like to acknowledge that the funding for this project was provided by a NASA Lunar Science Institute grant to UH administered by Dr. David Kring at the Lunar and Planetary Science Institute. I also want to thank my wife Haley and my dog Honey for loving me even when I was freaking out about finishing a paper on time or studying for an exam at the last minute, and for dealing with all my other ‘freak-out’ moments I had throughout this entire process. I could not have achieved this amazing accomplishment without their support and encouragement and for this I am eternally grateful.

**Lu-Hf and Sm-Nd Systematics of Apollo 17 Sample  
78236: Ages, Evolution and Investigations into the  
Neutron Fluence Correction on the Lu-Hf System**

---

An Abstract of a Thesis

Presented to

the Faculty of the Department of Earth and Atmospheric Sciences

University of Houston

---

In Partial Fulfillment

of the Requirements for the Degree

Master of Science

---

By

Samuel Tyer Simmons

December 2012

## Abstract

This thesis presents Lu-Hf, Sm-Nd, and Gd isotope and trace element concentration data of Apollo sample 78236,28. Apollo 17 sample 78236 was selected because it represents an early stage of lunar evolution. Sample 78236,28 yielded a 3-point neutron fluence bulk scale corrected Lu-Hf isochron age of  $4.418 \pm 0.022$  Ga,  $^{176}\text{Hf}/^{177}\text{Hf}$  initial of  $0.279706 \pm 0.000017$  ( $2\sigma$ ; MSWD = 1.7), a 3-point neutron fluence mineral scale corrected Lu-Hf isochron age of  $4.446 \pm 0.023$  Ga,  $^{176}\text{Hf}/^{177}\text{Hf}$  initial of  $0.279692 \pm 0.000017$  ( $2\sigma$ ; MSWD = 1.8), and a 5-point Sm-Nd isochron age of  $4.448 \pm 0.032$  Ga ( $2\sigma$ ; MSWD = 2.3) with an initial  $^{143}\text{Nd}/^{144}\text{Nd}$  ratio of  $0.507024 \pm 0.000038$ . Relative to chondritic uniform reservoir (CHUR) parameters of Bouvier et al. (2008), the  $\epsilon^{143}\text{Nd}_{(i)}$  and  $\epsilon^{176}\text{Hf}_{(i)}$  are  $+2.76 \pm 0.75$  and  $-6.71 \pm 0.69$ , respectively. Based on the measured data and model parameters, the uncorrected initial  $\epsilon^{176}\text{Hf}_{(i)}$ , using Lu-Hf CHUR parameters of Bizzarro et al. (2012), is  $-2.13 \pm 0.69$ . The apparent decoupling of the Nd and Hf initial isotope compositions may be indicative of system disturbance due to metamorphism, neutron capture effects, or perhaps related to uncertainties in applicable CHUR parameters. The Hf isotope data contain  $^{180}\text{Hf}$  isotope anomalies that are observed after mass bias correction using the exponential law. The measured isotope anomalies and modeling of neutron fluences indicate that neutron flux effects are a likely explanation for the observed Hf isotope data. The neutron fluences calculated by Edmunson et al. (2009) to correct their Sm-Nd data do not fully correct the Hf isotope data to natural values. In addition, the neutron fluences calculated from Sm and Gd isotope data measured in this study do not fully correct the Hf isotope data to natural values either. Based on neutron fluence modeling in this study, the fluences calculated from Sm and Gd data are likely a

product of a dwindling free neutron budget due to other neutron absorbers in the system. It is hypothesized that  $^{174}\text{Hf}$ ,  $^{176}\text{Hf}$ ,  $^{177}\text{Hf}$ ,  $^{178}\text{Hf}$ , and  $^{180}\text{Hf}$  demonstrated a greater sensitivity to free neutrons in the system than Sm or Gd, possibly due to absorption frequency overlap issues related to Fe and Ti in the sample.

# Contents

<b>1</b>	<b>Introduction</b>	<b>1</b>
<b>2</b>	<b>Sample Description</b>	<b>5</b>
<b>3</b>	<b>Analytical Methods and Sample Preparation</b>	<b>8</b>
<b>3.1</b>	<b>Sample preparation and <i>in situ</i> analysis</b>	<b>8</b>
<b>3.2</b>	<b>Sample digestion procedure for isotope analysis</b>	<b>10</b>
<b>3.3</b>	<b>Digestion procedure for trace element analysis</b>	<b>12</b>
<b>3.4</b>	<b>Mass spectrometry</b>	<b>12</b>
<b>3.4.1</b>	<b>ICP-MS trace element analysis</b>	<b>12</b>
<b>3.4.2</b>	<b>MC-ICP-MS isotope ratio analysis</b>	<b>15</b>
<b>3.5</b>	<b>Neutron fluence modeling</b>	<b>22</b>
<b>4</b>	<b>Results</b>	<b>28</b>
<b>4.1</b>	<b>Trace element analysis</b>	<b>28</b>
<b>4.2</b>	<b>Neutron fluence correction</b>	<b>31</b>
<b>4.3</b>	<b>Sm-Nd isotope data</b>	<b>37</b>
<b>4.4</b>	<b>Lu-Hf isotope data</b>	<b>40</b>
<b>5</b>	<b>Discussion</b>	<b>45</b>
<b>5.1</b>	<b>Modeled neutron fluence effects on Lu-Hf</b>	<b>45</b>
<b>5.2</b>	<b>Chronology of 78236</b>	<b>48</b>
<b>6</b>	<b>Conclusion</b>	<b>51</b>
	<b>References</b>	<b>53</b>

<b>Appendix I Neutron fluence model</b>	<b>57</b>
<b>Appendix II Sm-Nd neutron flux pathways</b>	<b>58</b>

## List of Figures

1	Mg-suite and FAN suite field classification	2
2	A. 78238,17 photomicrographs (XN)	7
	B. 78238,17 photomicrographs (reflected light)	7
3	Neutron flux effects based on temp	24
4	78236,28 REE spider-gram	29
5	78236,28 comparative trace element plot	30
6	Lu-Hf neutron flux pathways	31
7	Neutron flux effects based on Lu/Hf	34
8	$\epsilon^{180}\text{Hf}$ vs. $^{176}\text{Lu}/^{177}\text{Hf}$	35
9	Sm-Nd isochron	38
10	Nd mixing line	39
11	Lu/Hf uncorrected isochron & errorchron	42
12	Bulk corrected isochron	43
13	Mineral corrected isochron	44
14	$^{176}\text{Hf}/^{177}\text{Hf}$ evolution plot	50

## List of Tables

<b>1</b>	<b>Modal mineralogy of sample 78236</b>	<b>6</b>
<b>2</b>	<b>Trace element analysis</b>	<b>14</b>
<b>3</b>	<b>Lu-Hf data table</b>	<b>19</b>
<b>4</b>	<b>A. Sm data table</b>	<b>20</b>
	<b>B. Nd data table</b>	<b>20</b>
<b>5</b>	<b>Gadolinium data table</b>	<b>21</b>
<b>6</b>	<b>Epsilon Gd and <math>\epsilon^{180}\text{Hf}</math> anomalies</b>	<b>27</b>
<b>7</b>	<b>Bulk vs. mineral scale correction table</b>	<b>41</b>
<b>8</b>	<b>Table of published ages for sample 78236/ 8/ 5</b>	<b>49</b>

# List of Equations

<b>1 Neutron Fluence Equation</b>	<b>22</b>
-----------------------------------	-----------

---

# Chapter 1

## Introduction

The Moon is a planetary body whose early evolution may be analogous to the early differentiation processes of Earth and Mars (Hiesinger and Head 2006). Because the Moon preserves its differentiation history, lunar samples are important for constraining the processes and timescales of planetary differentiation (Hiesinger and Head 2006). The earliest periods of lunar magmatism are loosely understood, and have only recently begun to be unraveled by means of experimental petrology and geodynamic modeling (e.g. Elardo et al. 2011, Shearer and Papike 2005). To further understand these earliest events, constraining time periods for magmatism and source compositions of parent magmas is necessary. Radiogenic isotope systems, such as Sm-Nd, Lu-Hf, and Rb-Sr, have been used to date lunar samples and help constrain their source compositions. However, complications arise when looking at samples that have sustained intense bombardment and related thermal and shock metamorphism, subsequent alteration, and cosmic ray exposure. The Sm-Nd and Rb-Sr isotope systems have shown signs of disturbance due to these events throughout the Moon's history, which consequently may yield inaccurate ages and initial isotope ratios (Norman et al. 2003, Edmunson et al. 2009). These ages and ratios are essential for characterizing the source reservoirs and constraining the earlier magmatic history of the Moon.

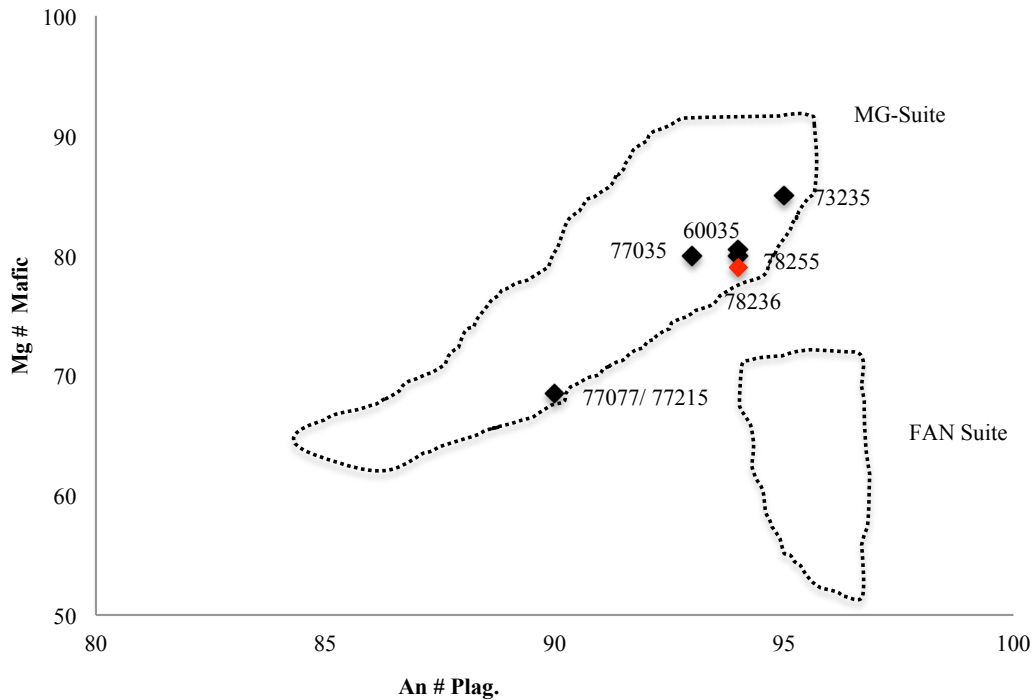


Figure 1. Figure displays the Mg-Suite and FAN suite classification fields. Sample used in this study in red.

The early (those occurring by 0 – 100 Ma after lunar formation) magmatic processes in the Moon produced two major igneous suites, the Mg-suite and the Ferroan Anorthosite, or FAN suite (Hiesinger and Head 2006). Relatively high Mg # of ~68-90 of olivine in conjunction with plagioclase having An contents of 85-95 and rock types ranging from troctolite to gabbro-norite characterize the Mg-suite. The ferroan anorthosite, FAN, suite is characterized by high An content of 90-98, Mg#s that range from ~50-70, and anorthosite as the dominant bulk lithology.

Apollo 17 sample 78236 is a nearly pristine Mg-suite norite (Figure 1; Edmunson et al. 2009 and references therein). Previous studies on 78235, 78236, and 78238, have produced ages and initial parent daughter ratios that show signs of disturbance due to impact events (Edmunson et al. 2009, Nyquist et al. 2008), and all of these sample aliquots originated from slightly different sections of the top of station 8 boulder. Edmunson et al. (2009) demonstrated that 78236 might represent one of the earliest occurrences of Mg-suite magmatism after the crystallization of the Lunar Magma Ocean (LMO), and could provide a more precise onset age of Mg-suite magmatism as well as answer some questions about the source composition for the entire Mg-suite.

A complication in understanding the age and initial isotope compositions measured on lunar samples is neutron capture reactions in materials exposed to cosmic rays. Rocks sitting at the surface of airless planetesimals are constantly subjected to irradiation (Lingenfelter et al. 1972, Hidaka et al. 2006, 2012) from cosmic ray exposure. Cosmic rays bombard atmosphere-less bodies, like the Moon, and irradiate the surface materials, which produce neutrons that are then absorbed by various isotopes (Hidaka et al. 2012, Eugster et al. 1970). The absorption of these neutrons can cause shifts in the isotope systems of the affected samples, and these shifts are important to consider because they can have profound affects on interpretations of ages an initial source compositions. In studies past, the convention to correct for this effect has been to use an isotope with a large capture window (neutron capture cross-section). The idea being, that this isotope can accurately represent the neutron flux in the system due to its maximized exposure to the neutrons in the system, thus allowing for adjustments to be made to other isotopes. The method to correct for these effects has not been developed specifically for

the Lu-Hf system and this thesis attempts to build on earlier work of Sprung et al. (2012) to understand neutron fluence effects on the Lu-Hf isotope system for lunar samples. After applying thermal neutron fluence corrections based on  $^{149}\text{Sm}$ , as is typically done to correct Nd isotopes, it is obvious that this will not be adequate to correct the effects on the Lu-Hf system in sample 78236,28, which is discussed in detail in section 3.5 and 4.2 of this thesis. The model developed in this thesis suggests that the correction factor produced from using  $^{149}\text{Sm}$  and  $^{157}\text{Gd}$  is too small and that a correction method utilizing Hf instead would be more ideal. Understanding the effects that thermal neutron fluence processes have had on the lunar surface is crucial in being able to use the Lu-Hf isotope system as another tool to understand the geologic history of the Moon. In samples of great antiquity, like 78236, even small adjustments can result in large corrections to ages and initials, and these values are crucial for developing an understanding of how the Moon evolved.

## Chapter 2

### Sample Description

#### 78236, 28:

Lunar sample 78236 is a highly shocked and nearly pristine Mg-suite norite (Blanchard et al. 1982). Its major element chemistry compared to other Mg-suite samples places it near the Mg-rich end-member of the suite, potentially representing the end of the LMO stage and the beginning of Mg-suite magmatism (Edmunson et al. 2009). The sample originated from the station 8 boulder that is described as small, ~ 0.5 meter diameter, and glass covered and was collected from atop the lunar regolith in the Sculptured Hills adjacent to the North Massif (Jackson et al. 1975). 78236 is composed of ~50% orthopyroxene and about ~50% plagioclase and contains trace amounts of clinopyroxene, Si-rich glass, phosphate minerals, potassium feldspar, baddelyite, zircon, troilite, ilmenorutile, ilmenite, chromite, and impact melt (Sclar and Bauer 1975; Dymek et al. 1975; McCallum 1975). The orthopyroxene grains are tabular with shock features including undulatory extinction, mosaicism, and planar deformation. The plagioclase is anorthite rich,  $An_{93-95}$  (Dymek et al. 1975, McCallum 1975), with a large percentage of the plagioclase converted to maskelynite. Overall, the sample is relatively friable due to the shock fracturing.

The allocated 1 g sample has a coarse grained surface that is visible on one side; the other side is coated in a black-gray glassy rind. The plagioclase in hand sample looks

opaque with a white-gray color. The pyroxenes appear to be interstitial and are a greenish yellow with some black oxides (Figure 2).

Samples	78235,6 <sup>a</sup>	78235,49 <sup>b</sup>	78236,8 <sup>c</sup>	78238 <sup>a,d</sup>
Opx.	51	51.2	53.6	32
Cpx.	0.01	0.01	0.6	<0.1
Plag.	48	48.2	39.2	68
High-Si Glass	0.25	0.25	2.4	Trace
K-Feld.	Trace		Trace	Trace
Phos.	0.03	0.032	Trace	Trace
Baddeleyite	Trace	Trace		Trace
Zircon	Trace	Trace		Trace
Troilite	Trace	Trace	Trace	
Ilmenorutile	Trace	Trace	Trace	Trace
Ilmenite				Trace
Chromite	Trace	Trace	Trace	Trace
Fe Metal	Trace	Trace	Trace	
Impact Melt			4	

Table 1. Modal mineralogy from thin section analysis reproduced from Edmunson et al (2009).

- A) James and Flohr (1983)
- B) McCallum and Mathez (1975)
- C) Nyquist et al. (1981)
- D) Unspecified thin sections

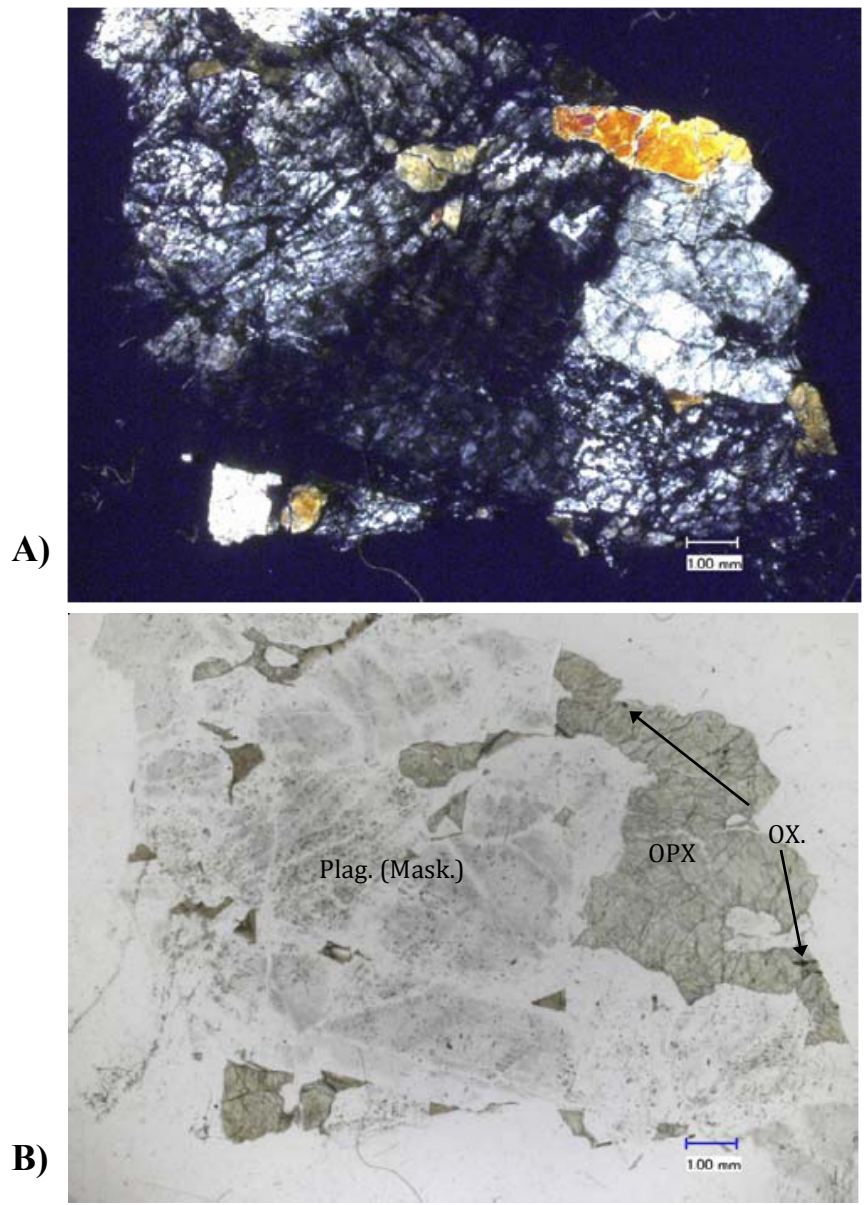


Figure 2. Photomicrographs of sample 78238,17. Has a representative composition and texture of sample 78236,28, which was used in this research. A) Refracted light, XP photomicrograph of 78238,17 from the Lunar Sample Compendium taken at 20x. B) Reflected light photomicrograph of 78238,17 from the Lunar Sample Compendium taken by Charles Meyer at 20x.

## Chapter 3

### Analytical Methods and Sample Preparation

#### 3.1 Sample preparation and *in situ* analyses

Apollo sample 78236,28 was disaggregated using a boron carbide mortar and pestle. The first stage was separating the fresh sample from the altered weathering rind. Once the rind was separated and removed, the sample was crushed repeatedly and sieved through a 3-stage nylon sieve. The sieve was thoroughly cleaned before use with DI water and ethanol. The sieve was triple graded using 100, 200, and 325 sized mesh screens. The 100-mesh screen is equivalent to 149 microns, the 200-mesh screen is equivalent to 74 microns and the 325-mesh screen is equivalent to 44 microns. The sieving process yielded sample cuts from each mesh size category and the >200 and >325 sized cuts were carried through 2 stages of heavy liquids, acetylene tetra-bromide and thallium malonate. The X > 200-mesh cut weighed 0.309 g and the X > 325-mesh cut weighed 0.23 g. The coarsest, X > 100 cut was repackaged and set aside, and the finest sized cut, X > 325, was used for the representative whole rock.

The X > 200 and X > 325-mesh sized cuts were separated using heavy liquids. Each sample cut was separated into 12-14 semi-even amounts, ~0.05 g to decrease the amount of sample going into each test tube in order to increase the effectiveness of the heavy liquids. The first stage of separation involved acetylene tetra-bromide (ATB) with a specific gravity of 2.85 g/cc. ATB effectively separates the plagioclase from the

heavier minerals in the sample. The second stage of separation involves thallium malonate with a specific gravity of 4.0 g/cc. Thallium malonate separates the pyroxene from the heaviest minerals. The different density cuts were then washed thoroughly and handpicked with a binocular microscope to ensure the highest purity. The representative 'whole rock' was weighed out from the  $X > 325$  mesh cut from the sieving process. After picking, clean plagioclase, clean pyroxene, dirty pyroxene (pyx. + ox.), and whole rock cuts were weighed.

Pyroxene and plagioclase grains were mounted in epoxy and analyzed by laser ablation (LA) ICPMS at the University of Houston in order to determine how much spike to add to the mineral separates. Ten grains from each mineral aliquot were analyzed with PhotonMachines Analyte.193 eximer laser ablation system coupled to a Varian 810 ICP-MS using a 50-micron spot size. Calcium-43 was used as an internal standard and the USGS basalt glass standard BHVO-2 was used as an external standard. Concentrations of Sm, Nd, Lu and Hf were calculated using the data reduction program GLITTER (Van Achterberg et al. 1999). Using the concentrations of Nd and Hf determined by LA-ICPMS and the sample weight of each sample fraction, the appropriate spike weight was calculated for each aliquot. This method, rather than citing previous works, insured proper sample/spike ratios for the different mineral separates used in this study.

### **3.2 Sample digestion procedure for isotope analysis**

**78236, 28:**

The mineral separates were measured out into ~50mg portions prior to being loaded into Parr high-pressure digestion vessels. Clean pyroxene weighed out to 55.4mg, clean plagioclase weighed out to 51.77mg, dirty pyroxene weighed out to 51.43mg, whole rock-A weighed out to 51.57mg, and dirty plagioclase weighed 53.85mg. The fractions, along with a procedural blank, were spiked with  $^{176}\text{Lu}$ - $^{178}\text{Hf}$  and  $^{149}\text{Sm}$ - $^{150}\text{Nd}$  mixed isotope tracers in 15ml FEP Savillex beakers. These fractions were combined with 4ml once distilled 29M HF and 0.5ml twice distilled 15M  $\text{HNO}_3$ , capped and heated for 24 hours at  $100^\circ\text{C}$  to pre-digest the silicates. The spiked sample fractions were dried down and brought back up in 3 ml 29M HF and 0.5 ml 14M  $\text{HNO}_3$  and transferred to PTFE teflon Parr<sup>TM</sup> bomb liners and placed in an oven where they were heated at  $150^\circ\text{C}$  for 72 hours. The samples were removed from the PTFE liners and placed in 15 ml Savillex beakers. The samples were dried and then brought back up in 4 ml 6M HCl until the solution was completely clear and there was no solid residue after centrifuging. This procedure ensures complete dissolution of the mineral fractions as well as complete spike sample equilibration.

Two additional whole rock samples were prepared in parallel with the other aliquots. 74.08mg of the >325 mesh fraction was digested following the methods outlined above but without the addition of spike. After digestion and full conversion to a clear solution in 6M HCl, the solution was split into two equal fractions each representing 37.04mg of whole rock. WR-1A and WR-2A underwent a “post-bombing” stage that

involved separately spiking WR-2A with  $^{176}\text{Lu}$ - $^{178}\text{Hf}$  and  $^{149}\text{Sm}$ - $^{150}\text{Nd}$  mixed isotope tracers; WR-1A remained unspiked. The WR samples were dried down to ensure spike sample equilibration of sample WR-2A as well as the consistency of the blank between the two samples. All of the sample solutions were then brought up in 6M  $\text{HNO}_3$  and transferred to the first round of ion exchange column chemistry.

The first stage of column chemistry uses anion resin in the Fe-removal process, which effectively removes nearly all Fe from the samples. The Hf was separated and purified from the REE and other matrix elements using a LN-Spec cation exchange resin following procedures outlined in Munker et al. (2001) and Lapen et al. (2004). Once Hf is removed, the remaining sample cut is transferred to Re-spec columns. The Re-spec column separates the REEs from the remaining elements. Samarium, Nd, Gd and Lu+Yb cuts were separated using  $\alpha$ -hydroxy-isobutaic (HIBA) acid with cation resin converted to  $\text{NH}_4^+$  form. After HIBA chemistry, all cuts are dried down and brought up in an Aqua Regia solution in order to dissolve the organic compounds left over from the HIBA. After removal of the organic residue, each dried sample cut was brought up in in a 2%  $\text{HNO}_3$  (Nd, Sm, Gd, and Lu+Yb) and 2%  $\text{HNO}_3$ -1% HF (Hf) and are ready for isotope analysis. All sample cuts were analyzed in house on the Nu-Plasma MC-ICPMS at 10ppb and 25ppb concentrations, depending on abundances of the element of interest.

### **3.3 Digestion procedure for trace element analysis**

A 16.05mg aliquot of the X > 325 mesh fraction was digested in a Parr bomb using 3ml of once distilled 29M HF, 1ml of twice distilled 15M HNO<sub>3</sub> and placed in an oven at 175° C for 48 hours. The procedural blank was prepared in an equal manner. After being heated for 48 hours, the solutions were transferred to Savillex beakers. The beakers were placed on the hot plate to dry down at 120° C for ~ 4 hours. One ml of ~ 6M HCl was added to the Savillex beakers after dry down and then they were capped, placed on the hot plate at 110° C and left for 24 hours in order to dissolve the fluoride salts. This process was repeated four times. The solution was then dried down and the residue was brought back up in 16.05g of 2% HNO<sub>3</sub>, which was weighed on the digital lab scale, and 0.160ml of multi-element spike was added to the sample. The sample and blank were analyzed on the Varian 810 ICP-MS system at the University of Houston following procedures outlined in Gao et al. (2009).

### **3.4 Mass spectroscopy**

#### **3.4.1 ICP-MS trace element analysis**

The 78236,28 and blank solutions were spiked using a multi-element spike containing precisely known concentrations of Rh, In, Tm, Re, Bi and enriched isotopes of <sup>6</sup>Li, <sup>61</sup>Ni, <sup>84</sup>Sr, and <sup>145</sup>Nd. The samples were then diluted with 18.2 MΩ water to a dilution factor of about 1000. The resulting solutions contain 2% HNO<sub>3</sub> and a nominal internal standard concentration of 10ppb. This multiple internal standards technique provides the ability to

monitor and correct the complex mass-dependent fractionations encountered in ICP-MS multi-element analysis. The sample and blank solutions were then analyzed on a Varian 810 quadrupole ICP-MS at the University of Houston. The data reduction process corrects for machine drift using combined internal and external standards. Prior to the run, a 5ppb solution of pure Nd is analyzed in order to correct for oxide interferences with the REE's, Hf and Ta as reported in Gao et al. (2009). Typical analytical precision as reported by Gao et al. (2009) is less than 5% ( $2\sigma$ ) for the elements measured, which is represented by the relative standard deviation (Table 2).

<b>weight (ppm)</b>	<b>78236,28 This Study (2012)</b>	<b>Blanchard (1981)</b>	<b>Nyquist (1981)</b>
<i>Element</i>			
Li	6.23	-	-
Be	0.88	-	-
B	319	-	-
Sc	9.99	11.2	-
Ti	903	-	-
V	65.6	-	-
Cr	1949	2120	-
Mn	878	-	-
Co	16.14	28.2	-
Ni	24.82	-	-
Cu	3.38	-	-
Zn	4.84	-	-
Ga	3.15	-	-
Rb	0.89	-	0.862
Sr	106	-	104
Y	17.3	-	-
Zr	62.2	-	-
Nb	6.67	-	-
Cs	0.06	-	-
Ba	73.4	-	-
La	5.52	4.47	-
Ce	14.12	12.8	-
Pr	1.95	-	-
Nd	8.31	-	7.02
Sm	2.31	1.93	2
Eu	0.89	0.82	-
Gd	2.69	-	-
Tb	0.47	0.53	-
Dy	3.11	-	-
Ho	0.66	-	-
Er	1.93	-	-
Yb	1.88	2.12	-
Lu	0.26	0.32	-
Hf	1.53	1.7	-
Ta	0.28	0.2	-
Pb	0.77	-	-
Th	0.82	0.6	-
U	0.3	-	-

*ICP-MS*

*INAA*

*IDMS*

Table 2. Trace element analysis comparison of this study and two previous studies. Comparison is good between the data sets, although the newer data set is much more extensive.

### 3.4.2 MC-ICP-MS isotope ratio analyses

The Hf cuts were prepared in 500 $\mu$ l of 2% HNO<sub>3</sub>-1% HF and placed on the hot plate overnight to ensure complete dissolution. Ten microliters of the sample was then diluted with 490 $\mu$ l of 2% HNO<sub>3</sub>-1% HF and run for a pre-concentration test in order to determine how to properly dilute each individual sample for analysis. Hafnium cuts were diluted to 10ppb and 25ppb concentrations depending on abundance of Hf in the sample.

The Lu, Sm, Nd, and Gd cuts were prepared in 500 $\mu$ l of 2% HNO<sub>3</sub> solution and placed on a hot plate to ensure complete dissolution of the sample. Once completely dissolved, 10 $\mu$ l of sample solution was added to 490 $\mu$ l of the 2% HNO<sub>3</sub> solution and run on the MC-ICPMS for a pre-concentration test in order to know how to properly dilute each sample. Each sample was then properly diluted to 10ppb and 25ppb, depending on the pre-concentration test, and run on the MC-ICPMS. All isotopes were analyzed on a Nu-Plasma II using a Cetac Aridus II nebulizer.

Spiked Hf samples are mass bias corrected and spike subtracted based on methods outlined in Lapen et al. (2004), where samples are bracketed by standards. The sample standard bracketing method allows for a linear mass bias correction coefficient to be calculated relative to the true values of the standards, which is used to modify the exponential correction method (Lapen et al. 2004). Isobaric interferences from <sup>176</sup>Yb and <sup>176</sup>Lu on <sup>176</sup>Hf and <sup>180</sup>W and <sup>180</sup>Ta on <sup>180</sup>Hf are removed by following procedures outlined in Lapen et al. (2004).

Lapen et al. (2004) developed this method because they observed that the use of an exponential law alone to correct spiked Hf samples would consistently fail to produce data with external precision that was equivalent to the unspiked samples.

The unspiked Hf samples can be corrected using internal normalization to  $^{179}\text{Hf}/^{177}\text{Hf} = 0.7325$ , while using an exponential law combined with a linear correction method that utilizes the offset of exponentially corrected data to the true value of the standards (Lapen et al. 2004). These methods outlined for Hafnium samples are applicable to the Sm, Nd systems as reported by Lapen et al. (2004). In the Sm-Nd system we monitor isobaric interference from  $^{142}\text{Ce}$ ,  $^{144}\text{Sm}$ ,  $^{148}\text{Sm}$ , and  $^{150}\text{Sm}$  on Nd and we monitor  $^{144}\text{Nd}$ ,  $^{148}\text{Nd}$ ,  $^{150}\text{Nd}$ ,  $^{152}\text{Gd}$ , and  $^{154}\text{Gd}$  interferences on Sm.

The  $^{176}\text{Hf}/^{177}\text{Hf}$  operating values measured for internal laboratory standards during run 1 (samples 12HN19, 12HN20, 12HN21 & 12HN22) are; UH Ames 25ppb Hf  $0.282358 \pm 0.000002$  ( $2\sigma$ ) ( $n = 7$ ), UWisconsin JMC 475 25ppb Hf  $0.282163 \pm 0.000025$  ( $2\sigma$ ) ( $n = 5$ ), PlasmaCal 25ppb Hf  $0.282156 \pm 0.000018$  ( $2\sigma$ ) ( $n = 6$ ) and run 2 (samples 12HN25 & 12HN29) are; UH Ames 25ppb Hf  $0.282359 \pm 0.000025$  ( $2\sigma$ ) ( $n = 7$ ), UWisconsin JMC 475 25ppb Hf  $0.282163 \pm 0.000025$  ( $2\sigma$ ) ( $n = 5$ ) and UH JMC 475 25ppb Hf  $0.282196 \pm 0.000028$  ( $2\sigma$ ) ( $n = 42$ ). In the age calculations for the two isochrons I used external error values of  $\pm 0.005\%$  for the  $^{176}\text{Hf}/^{177}\text{Hf}$  ratios and  $\pm 0.2\%$  for the  $^{176}\text{Lu}/^{177}\text{Hf}$  ratios, which are based on long-term reproducibility of pure Hf standard solutions and USGS rock standards. Our UWisc. JMC 475 standards produce identical values to those published in Blichert-toft (2001). The  $^{143}\text{Nd}/^{144}\text{Nd}$  ratio measured for internal laboratory standards in run 1 are; UH Ames 25 ppb Nd  $0.511979 \pm 0.000024$  ( $2\sigma$ ) ( $n = 47$ ) and Jndi 25ppb Nd  $0.512105 \pm 0.000010$  ( $2\sigma$ ) ( $n = 7$ ) and run 2 are; UH Ames 25ppb Nd  $0.511979 \pm 0.000025$  ( $2\sigma$ ) ( $n = 47$ ) and Jndi 25ppb Nd  $0.512102 \pm 0.000023$  ( $2\sigma$ ) ( $n = 7$ ). All  $^{147}\text{Sm}/^{152}\text{Sm}$  and  $^{143}\text{Nd}/^{144}\text{Nd}$  ratios of standards and samples were corrected for instrumental mass bias using the same methods outlined

by Lapen et al. (2004) for Sm, Nd, Lu & Hf correction. All age calculation for the Sm-Nd isochron used external reproducibility errors of 0.003% ( $2\sigma$ ) for  $^{143}\text{Nd}/^{144}\text{Nd}$  and 0.2% ( $2\sigma$ ) for  $^{147}\text{Sm}/^{144}\text{Nd}$ .

Gadolinium data was corrected using the exponential law as well as an isobaric correction for  $^{158}\text{Dy}$  and  $^{160}\text{Dy}$ . The correction method utilized the  $^{(155+156)}\text{Gd}$  value developed in Hidaka et al. (2000) to eliminate the  $^{160}\text{Dy}$ , and create a beta value for  $^{155}\text{Gd}$ ,  $^{156}\text{Gd}$ ,  $^{157}\text{Gd}$ , and  $^{158}\text{Gd}$  in order to carry out the exponential correction. The beta value is calculated based on a  $^{(155+156)}\text{Gd}/^{160}\text{Gd}$  ratio in order to account for  $^{155}\text{Gd}$  lost to neutron fluence effects. Since  $^{156}\text{Gd}$  has such a small cross-section the sum of  $^{(155+156)}\text{Gd}$  is essentially constant and can be used for the mass bias correction. The  $^{155}\text{Gd}/^{160}\text{Gd}$ ,  $^{156}\text{Gd}/^{160}\text{Gd}$ ,  $^{157}\text{Gd}/^{160}\text{Gd}$ , and  $^{158}\text{Gd}/^{160}\text{Gd}$  operating values measured for internal laboratory standards during runs were; PlasmaCal 15ppb Gd  $0.676119 \pm 0.000033$ ,  $0.935175 \pm 0.000033$ ,  $0.715535 \pm 0.000054$  &  $1.135529 \pm 0.000106$  ( $2\sigma$ ) respectively, ( $n = 13$ ). All Gd isotope standard ratios are reported because the Gd was unspiked.

The Lu, Sm, Nd, and Gd cuts were prepared in 500 $\mu\text{l}$  of 2%  $\text{HNO}_3$  solution and placed on a hot plate to ensure complete dissolution of the sample. Once completely dissolved, 10 $\mu\text{l}$  of sample solution was added to 490 $\mu\text{l}$  of the 2%  $\text{HNO}_3$  solution and run on the MC-ICP-MS for a pre-concentration test in order to know how to properly dilute each sample. Each sample was then properly diluted to 10ppb and 25ppb, depending on the pre-concentration test, and run on the MC-ICPMS. The measured Lu data was reduced in excel form to correct for isobaric interference from  $^{176}\text{Yb}$  and  $^{176}\text{Hf}$  isobars and instrumental mass fractionation following methods outlined in Lapen et al. (2004). All isotopes were analyzed on a Nu-Plasma II using a Cetac Aridus II nebulizer.

An additional neutron fluence correction was required using  $^{149}\text{Sm}$  for the Lu/Hf isotope system.  $^{149}\text{Sm}$  is an ideal candidate for neutron fluence corrections because the neutron capture cross-section is one of the most sensitive to thermal neutrons of all the elements being analyzed (Hidaka et al. 2006, Brandon et al. 2009, Edmunson et al. 2009, Hidaka et al. 2010). The measured Lu data were reduced in an excel spreadsheet following methods outlined in Vervoort et al. (2004). Table 3, Table 4A and 4B and Table 5 on the following pages list the results of 78236,28 for Sm-Nd, Lu-Hf and Gd from the MC-ICP-MS.

Sample #	Type	Wt (g)	Lu ppm	Hf ppm	$^{176}\text{Lu}/^{177}\text{Hf}$	$^{176}\text{Lu}/^{175}\text{Lu}$	$^{176}\text{Hf}/^{177}\text{Hf}$	$^{178}\text{Hf}/^{177}\text{Hf}$	$^{180}\text{Hf}/^{177}\text{Hf}$
12HN19 b	WR	0.05157	0.05	1.79	0.039521	0.1022591 ± 225	0.2817911 ± 14	2.06481 ± 23	1.86064 ± 53
12HN20 a	PLAG.	0.05368	0.44	0.56	0.011987	0.1131957 ± 199	0.2807412 ± 17	1.70036 ± 39	1.87635 ± 44
12HN21 c	PYX.	0.05580	0.49	1.18	0.060599	0.1424479 ± 105	0.2849206 ± 14	3.12642 ± 74	1.81583 ± 58
12HN22 d	PYX. + OX.	0.05153	0.51	2.29	0.032295	0.1483031 ± 58	0.2824749 ± 18	2.30636 ± 53	1.85032 ± 63
12HN25 e	PLAG. + OX.	0.05385	0.07	1.74	0.001427	0.1444938 ± 143	0.2803636 ± 15	1.61494 ± 37	1.88050 ± 62
12HN28	WR(UNSP.)	0.03704	-	-	-	0.0250682 ± 39	0.2818358 ± 16	1.81666 ± 97	1.87198 ± 59
12HN29	WR	0.05157	0.32	2.29	0.020325	0.1420071 ± 79	0.2816624 ± 16	1.99654 ± 61	1.86402 ± 58

Table 3. Lu-Hf data table. Errors =  $2\sigma$  abs. from in-run statistics. Letters correspond to points on the isochrons.

Sample #	Type	Wt (g)	Sm ppm	$^{147}\text{Sm}/^{144}\text{Nd}$	$^{148}\text{Sm}/^{152}\text{Sm}$	$^{149}\text{Sm}/^{152}\text{Sm}$	$^{150}\text{Sm}/^{152}\text{Sm}$	$^{154}\text{Sm}/^{152}\text{Sm}$
12HN19 b	WR	0.05157	1.178667131	0.160473	0.4191611 ± 25	6.875618 ± 590	0.2809433 ± 9	0.8500684 ± 71
12HN20 a	PLAG.	0.05368	0.686384308	0.139185	0.4184175 ± 33	10.21376 ± 126	0.2819245 ± 13	0.8493213 ± 85
12HN21 c	PYX.	0.05580	0.450724715	0.244183	0.4197308 ± 23	4.026106 ± 194	0.2800778 ± 10	0.8504985 ± 61
12HN22 d	PYX. + OX.	0.05153	0.682341915	0.202348	0.4199861 ± 17	2.816582 ± 85	0.2797079 ± 8	0.8506332 ± 84
12HN25 e	PLAG. + OX.	0.05385	2.052434645	0.142508	0.4198126 ± 49	3.406160 ± 243	0.2786471 ± 19	0.8501770 ± 121
12HN28	WR(UNSP.)	0.03704	-	-	0.4204916 ± 36	0.513906 ± 67	0.2789554 ± 19	0.8506566 ± 100
12HN29	WR	0.05157	1.919469098	0.167989	0.4197920 ± 42	4.018214 ± 342	0.2787145 ± 22	0.8504941 ± 122

Sample #	Type	Wt (g)	Nd ppm	$^{143}\text{Nd}/^{144}\text{Nd}$	$^{145}\text{Nd}/^{144}\text{Nd}$	$^{146}\text{Nd}/^{144}\text{Nd}$	$^{148}\text{Nd}/^{144}\text{Nd}$	$^{150}\text{Nd}/^{144}\text{Nd}$
12HN19 b	WR	0.05157	4.258286995	0.5117443 ± 88	1.141502 ± 19	0.3484437 ± 54	0.2425108 ± 61	0.7996060 ± 252
12HN20 a	PLAG.	0.05368	2.858618711	0.5111329 ± 97	1.141626 ± 20	0.3485124 ± 48	0.2428029 ± 59	0.9899434 ± 298
12HN21 c	PYX.	0.05580	1.070764032	0.5142393 ± 79	1.141623 ± 19	0.3484420 ± 49	0.2423390 ± 42	0.7045302 ± 192
12HN22 d	PYX. + OX.	0.05153	1.955577526	0.5129928 ± 71	1.141680 ± 19	0.3484115 ± 51	0.2419707 ± 48	0.4899938 ± 154
12HN25 e	PLAG. + OX.	0.05385	8.3205	0.5112448 ± 74	1.141842 ± 20	0.3484060 ± 44	0.2419761 ± 53	0.4424298 ± 131
12HN28	WR(UNSP.)	0.03704	-	0.5120199 ± 65	1.141829 ± 19	0.3484151 ± 42	0.2416068 ± 53	0.2361742 ± 77
12HN29	WR	0.05157	6.6	0.5120247 ± 78	1.141835 ± 21	0.3484093 ± 46	0.2421663 ± 54	0.5313120 ± 160

Table 4A. Sm data table. Errors = 2σ abs. from in-run statistics 4B.  
Nd data table. Errors = 2σ abs. from in-run statistics. Letters correspond to points on the isochrons.

Sample #	Type	Wt (g)	Gd ppm	$^{155}\text{Gd}/^{160}\text{Gd}$	$^{156}\text{Gd}/^{160}\text{Gd}$	$^{157}\text{Gd}/^{160}\text{Gd}$	$^{158}\text{Gd}/^{160}\text{Gd}$
12HN19	WR	0.05157	-	0.6753438 ± 40	0.9359431 ± 40	0.7120701 ± 52	1.138862 ± 11
12HN20	PLAG.	0.05368	-	0.6754287 ± 39	0.9358573 ± 40	0.7120347 ± 60	1.138882 ± 9
12HN21	PYX.	0.05580	-	0.6753681 ± 48	0.9359199 ± 47	0.7120821 ± 76	1.138939 ± 10
12HN22	PYX. + OX.	0.05153	-	0.6753578 ± 43	0.9359306 ± 43	0.7120947 ± 65	1.138939 ± 78
12HN28	WR(UNSP.)	0.03704	-	0.6754132 ± 57	0.9358738 ± 57	0.7121647 ± 76	1.138939 ± 10
12HN29	WR	0.05157	-	0.6753748 ± 52	0.9359231 ± 51	0.7120465 ± 65	1.138939 ± 10

Table 5. Gd data table. Errors =  $2\sigma$  abs. from in-run statistics

### 3.5 Neutron fluence modeling

Sample 78236 was observed to have a positive  $^{178}\text{Hf}$  and a negative  $^{180}\text{Hf}$  isotope anomaly, which can be indicative of neutron flux effects (e.g. Nyquist et al. 1995). As cosmic rays interact with the surfaces of atmosphere-less terrestrial bodies reactions take place that produce neutrons (Lingenfelter 1972, Hidaka et al. 2008 and references therein). These neutrons then interact with different elements and are eventually absorbed. When neutrons are absorbed by an atomic nucleus it cause then atomic weight to increase. These shifts in isotopic system can have profound effects during the data reduction processes causing skewed ages and initial values which in turn effect our interpretations of the data. The rate that isotopes absorb free neutrons can be dependent on the temperature of the reactions taking place. To determine the temperature range for the neutron-fluence reactions, a model was constructed. The model utilized a database from the National Nuclear Data Center developed by Brookhaven National Labs that relied on ENDF/B V. II.0-II.1 codes to provide cross section variation with respect to energy for all isotopes involved in the Sm-Nd and Lu-Hf decay schemes. Lists for all isotopes from Yb, Lu, Hf, Sm, Gd, and Eu were collected and processed through a program developed by Rasmus Andreasen. This program uses the cross section sizes as they vary with energy level, along with a manual temperature input from the user, to integrate the area underneath the frequency curve produced. The area underneath the curve represents the cross section area at a particular temperature. Cross sections were calculated for all isotopes of Yb, Lu, Hf, Sm, Gd, and Eu at temperatures ranging from 20 K to 520 K, the idea being that this temperature range would encompass temperatures

experienced on the Moon as cited by Hidaka et al. (2006) and Lingenfelter (1972). Once cross section sizes were established for the aforementioned temperature ranges, the data were input back into the model. The result was concentrations that were produced by neutron flux for all significant isotopes of Yb, Lu, Hf, Sm, Gd, and Eu assuming a psi,  $\Psi$ , value calculated using:

$$\Psi = -1.0 \times 10^{-4} \epsilon_{149\text{Sm}} / \sigma_{149} \quad (1)$$

from Hidaka et al. (2000) where  $\sigma_{149}$  is the effective thermal neutron capture cross section in  $\text{cm}^2$ . These data were run through the mass bias correction used to correct for instrumental mass fractionation. Based on the modeling,  $^{177}\text{Hf}$  is the most susceptible of the Hf isotopes to neutron capture effects, and it is also the normalizing isotope. Thus, coupled anomalies in  $^{177}\text{Hf}$  and  $^{178}\text{Hf}$  will affect the accuracy of the mass bias correction and isotope dilution calculations, respectively. Modeling of the predicted isotope shifts related to neutron fluence effects in mass-bias corrected data utilizes the ‘normal’  $^{179}\text{Hf}/^{177}\text{Hf}$  of 0.7325 (set to zero in Figure 3 below). The mass bias corrected model data were plotted for each isotope vs. the deviation from ‘truth’ in epsilon notation of each along with the measured data from the unspiked sample. The result of the modeling was a strong correlation with the patterns seen in the model compared to the pattern experienced by the sample (Figure 3).

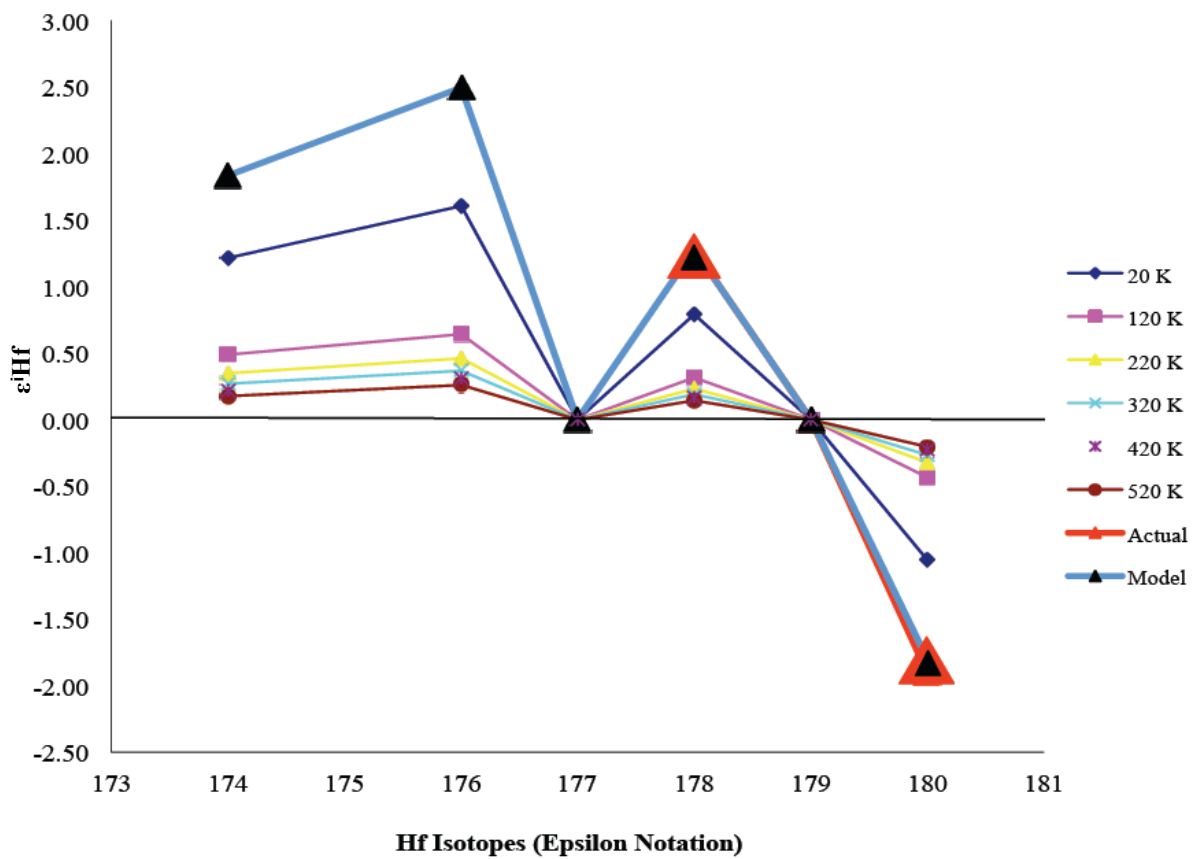


Figure 3. Displays the results of the temperature model on the Hf isotopes and how the results compare with the actual data (Bright Blue Rectangles). The “Model” curve fits the actual data exactly, with in error, and was calculated by increasing the fluence factor on the 20 K trend by an arbitrary factor until the fit was achieved.

The modeled data show that the neutron absorption experienced by 78236 follows a near identical pattern to the model predicted results. The pattern displayed by the actual measured data plots very similarly to the modeled data, except that the measured data are more elevated than the 20 K modeled data. We observed in the modeling that as neutron fluence increased the temperature decreased, but in order to achieve a model pattern that fit the actual data an unrealistic surface temperature of 0 K-10 K would be required. This suggested that the absorption sensitivities of the Hf isotopes were likely higher than originally predicted rather than the temperature being colder. In the modeled data I observed the pattern, between isotopes, of the model curve did not vary with increasing temperature which made it difficult to constrain the temperature of the 78236,28 system at such low Lu/Hf ratios. Model parameters and constructions can be found in *Appendix I*.

All data collected by the MC-ICPMS have to go through an instrumental mass bias correction, spike subtraction (for spiked samples), and isotope dilution calculation procedure (e.g. Lapen et al. 2004) in order to obtain corrected isotope data and element concentrations as explained in section 3.4.2 of this thesis. The difficulty arose when doing the mass bias correction because of neutron capture reactions (Lingenfelter et al. 1972, Hidaka et al. 2000, 2006, 2012, Brandon et al. 2009 and Edmunson et al. 2009). This effect has produced coupled over and under abundances of ( $^{178}\text{Hf} = +1.23$  epsilon units and  $^{180}\text{Hf} = -1.9$ , and a calculated  $+2.49 \pm 0.5$  epsilon shift in  $^{176}\text{Hf}$ ; Figure 3) isotopes used in the mass bias corrections subsequently skewing the mass bias corrected values for  $^{176}\text{Hf}$ . The  $^{176}\text{Hf}$  shift was calculated by using the product of the measured  $^{178}\text{Hf}$  and  $^{180}\text{Hf}$  anomalies as well as the modeled  $^{176}\text{Hf}/^{177}\text{Hf}$  shift. Because  $^{149}\text{Sm}$  has the

second largest neutron capture cross section for thermal neutrons, we attempted to use the neutron flux calculated from offsets in the abundance of  $^{149}\text{Sm}$  (e.g. Hidaka et al. 2000 and references therein). In addition to possessing a large capture cross section, the  $^{149}\text{Sm}$  isotope is a strong non- $1/v$  isotope similar to  $^{176}\text{Lu}$  (Parrington, John R. Nuclides and Isotopes, 15<sup>th</sup> ed.), which means the behavior of the cross section size with respect to temperature might be similar, making  $^{149}\text{Sm}$  an ideal isotope to correct the effects on the Lu-Hf system, assuming that Lu has a significant input into Hf. Although the magnitude of a neutron fluence correction based on the neutron flux calculated from shifts in  $^{149}\text{Sm}$  abundances was too small based on modeled  $^{180}\text{Hf}$  anomalies compared to measured anomalies in the unspiked sample, the ratio of the change between isotopes remain constant since our measured data fit the modeled data pattern (Figure 3). The mass-biasing problem has affected the  $^{176}\text{Hf}/^{177}\text{Hf}$  values of the isochron by a magnitude of about  $+2.49 \pm 0.5$  epsilon units and must be corrected for in 78236,28 before the age and initial Hf isotope composition can be fully interpreted.

The robustness of this result requires an evaluation of some of the starting parameters of the model. First, the starting isotope composition of Hf was investigated as to whether or not the starting Hf composition had an effect on the fluence correction. Hf isotope abundances were calculated for  $\epsilon^{176}\text{Hf}$  ranging between -75 to +120 relative to the CHUR values. The modeled result indicates that no matter how evolved or primitive the starting composition was, the fluence model values did not result in a change in the mass-bias corrected Hf isotope ratios. The second test of model parameters was to investigate whether the  $^{176}\text{Lu}/^{177}\text{Hf}$  ratio had any effect on the fluence correction (we had initially assumed it was not based on the constant  $^{(155,156,157,158)}\text{Gd}$  and  $^{180}\text{Hf}$  anomalies we

observed across all samples; Table 6). The Lu/Hf ratio was varied from 0.1 to 5 times the original  $^{176}\text{Lu}/^{177}\text{Hf}$  ratio and the temperature for the neutron capture reactions was varied from 20 K to 520 K. The temperature variation was necessary because of the non- $1/v$  nature of  $^{176}\text{Lu}$ . The effect that changing the Lu/Hf ratio had on Hf abundances was then modeled from the data and is discussed in section 4.2 (Figure 7).

	$\epsilon^{155}\text{Gd}$	$\epsilon^{156}\text{Gd}$	$\epsilon^{157}\text{Gd}$	$\epsilon^{158}\text{Gd}$	$\epsilon^{180}\text{Hf}$
12HN19 Gd	$-11.32 \pm 0.49$	$8.09 \pm 0.36$	$-48.32 \pm 0.76$	$29.67 \pm 0.93$	$-1.50 \pm 0.34$
12HN20 Gd	$-10.09 \pm 0.49$	$7.21 \pm 0.36$	$-48.71 \pm 0.76$	$29.66 \pm 0.93$	$-1.21 \pm 0.34$
12HN21 Gd	$-11.06 \pm 0.49$	$7.86 \pm 0.36$	$-48.43 \pm 0.76$	$29.93 \pm 0.93$	$-1.51 \pm 0.34$
12HN22 Gd	$-11.26 \pm 0.49$	$8.02 \pm 0.36$	$-48.20 \pm 0.76$	$30.21 \pm 0.93$	$-1.62 \pm 0.34$
12HN28 Gd	$-10.73 \pm 0.49$	$7.67 \pm 0.36$	$-48.16 \pm 0.76$	$29.51 \pm 0.93$	$-1.64 \pm 0.14$
12HN29 Gd	$-11.21 \pm 0.49$	$7.89 \pm 0.36$	$-49.43 \pm 0.76$	$28.35 \pm 0.93$	$-2.36 \pm 0.14$

Table 6. Table showing epsilon values for samples run in this study. Important to note that they are all consistent from mineral to mineral. Error is  $2\sigma$ .

## Chapter 4

### Results

#### 4.1 Trace element analyses

There are inherent challenges in obtaining representative isotopic and element concentration data from small samples of coarse-grained rocks. One method of obtaining representative composition data is to invert *in situ* element data of constituent phases. The disadvantages to this method are the assumptions that all constituent phases are recognized, that the average compositions of the constituent phases can be measured, and the mineral mode is accurately measured. In many cases, these assumptions are not valid, in particular if there are minor phases in the rock that are rich in a particular element or groups of elements (e.g. phosphate minerals with respect to REE). For the sample studied here, the friable nature of the sample yielded powder (> 325 mesh) during disaggregation that we interpret as a representative fraction of the 1.0g mass of the sample. Another test of this interpretation is to compare our data with INAA data previously determined for 78236,28 (Blanchard et al. 1982). Overall, there is excellent agreement between the two analyses and both exhibit small to unresolvable positive Eu anomalies (Figure 4). Figure 5 shows comparisons between other Mg-suite norites and granulites in order to recognize materials that may be genetically related and guide future isotopic studies to test these connections.

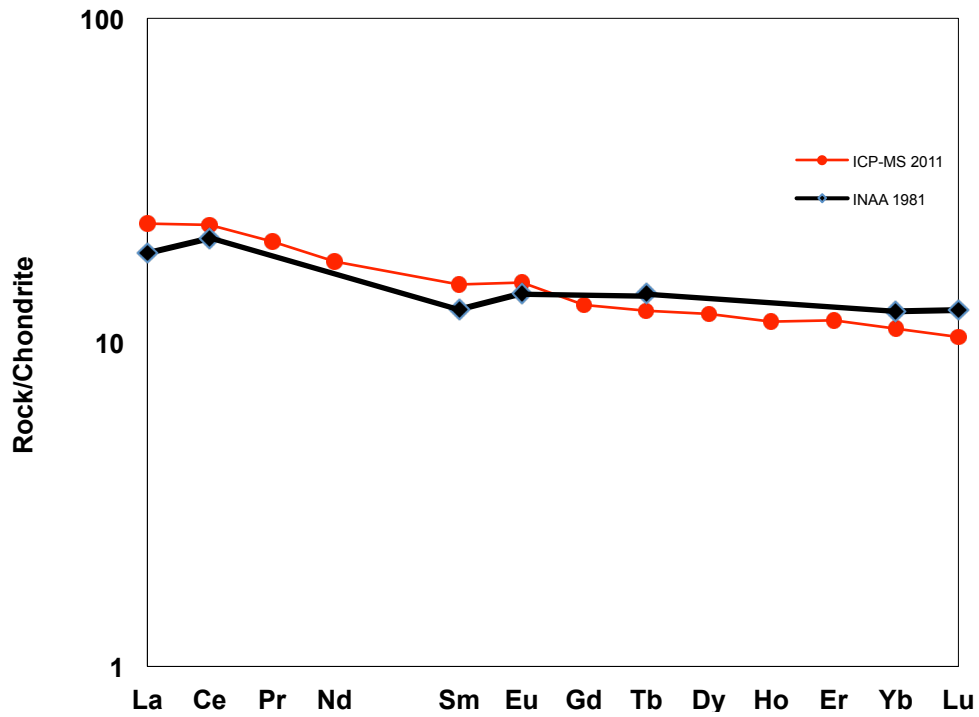


Figure 4 Rare Earth Element plot for Apollo 17 sample 78236. Red circles are ICP-MS data gathered in house at the University of Houston for this study. Black diamonds represent INAA data collected by Blanchard et al. (1981). There is an excellent resemblance in the two sets of data, which validated the results for this study.

\* Lines were extrapolated between data points in the black pattern to account for missing data, similar to the chart found in the Lunar Sample Compendium compiled by C. Meyer.

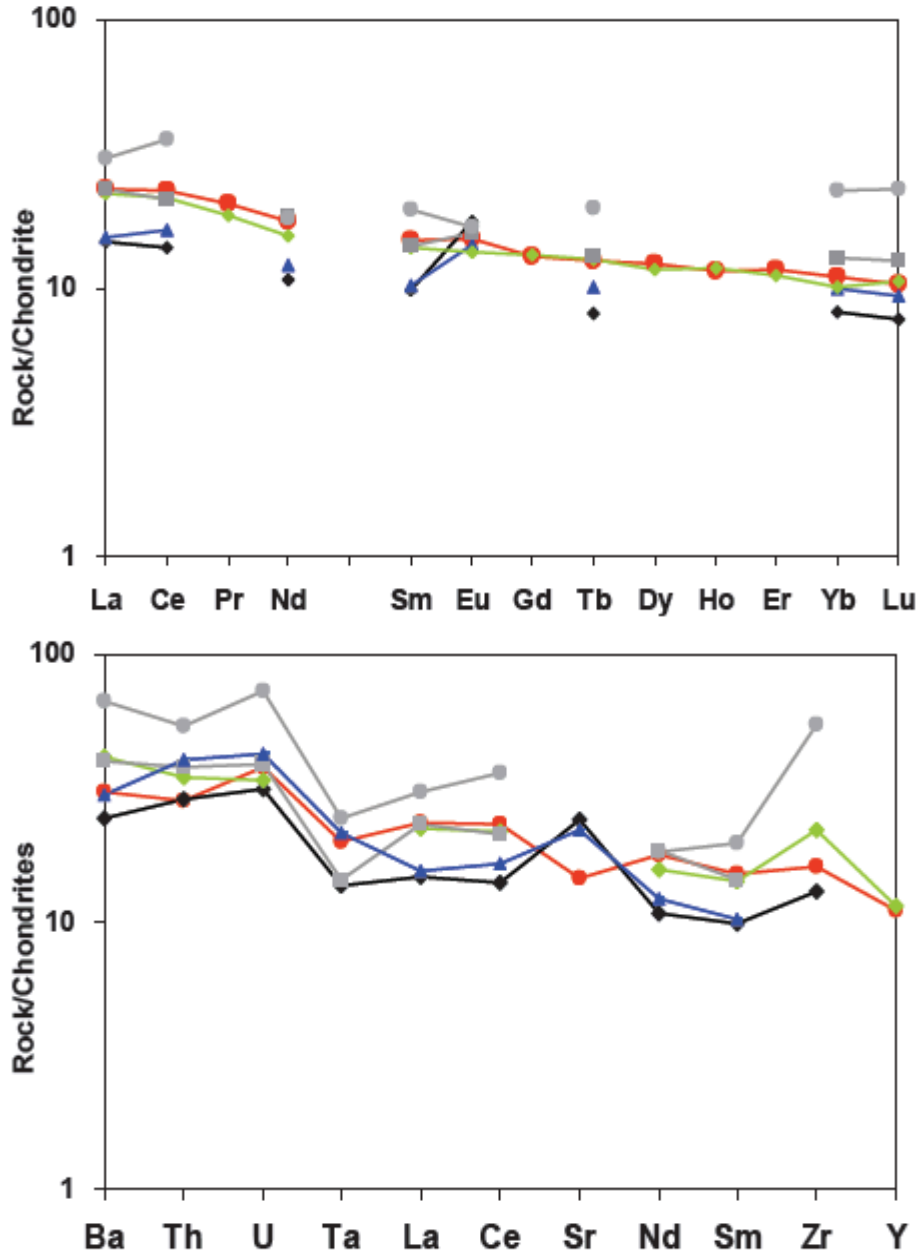


Figure 5 Top: Chondrite-normalized rare earth element (REE) abundances in 78236 (this study), 60035 (black diamond), 72275 (blue triangle), 73235 (green diamond), 77035 (gray square), 77075 (gray circle). See text for details of what portions of each sample are presented. It is notable that 73235 and 77035 have nearly identical REE abundances to 78236.

Bottom: Chondrite-normalized trace element abundances for the samples listed in the top diagram. Coloring scheme is also identical to the above. As shown by the REE data, 73235 and 77035 also have abundances of trace elements that are identical to 78236.

## 4.2 Neutron-fluence correction

The neutron-flux correction significantly affected  $^{177}\text{Hf}$  and  $^{178}\text{Hf}$ . Hf isotopes, in general, were largely unaffected by the neutron capture on Lu given the low Lu/Hf ratios analyzed.

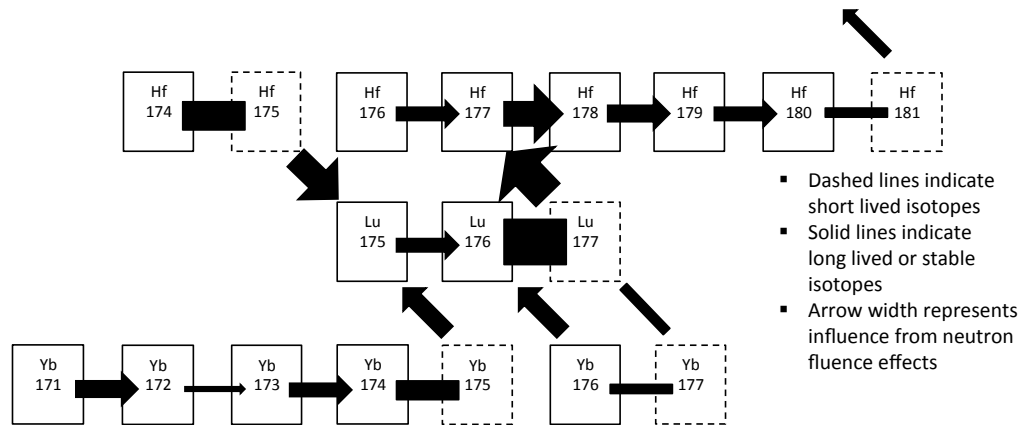


Figure 6. Figure showing scaled neutron flow paths through the Lu-Hf system.

The figure represents the flow paths influenced by neutron-flux in the Lu-Hf system. There is a major input from  $^{176}\text{Lu}$  because the capture cross-section for  $^{176}\text{Lu}$  is relatively large. Hf, however, does not feel these effects, as mentioned earlier and so Hf capture tends to behave like a closed system in 78236,28. This means that the effect in Hf is  $^{177}\text{Hf} \rightarrow ^{178}\text{Hf}$ .

The results of the modeling for sample 78236,28 predicted a shift in  $^{176}\text{Hf}$  by  $+2.49 \pm 0.5$  epsilon units for 12HN20, 12HN21, and 12HN22, and a shift of  $+3.19 \pm 0.5$

epsilon units for samples 12HN25 and 12HN29. While the shift in the two samples that fell off the isochron, 12HN25 and 12HN29, was not enough to realign them with the other three data points, the correction did shift the other three data points an equal amount. The shift in data produced an initial  $^{176}\text{Hf}/^{177}\text{Hf}$  value that was more subchondritic than originally calculated, but due to the heightened sensitivity of  $^{176}\text{Hf}$  there is an error of  $\pm \sim 0.5$  epsilon units in addition to the measured error. The error was determined by assessing the difference between the minimum and maximum epsilon shifts on the  $^{176}\text{Hf}$  calculated from  $^{178}\text{Hf}$  and  $^{180}\text{Hf}$  anomalies.

When considering the fluence effect on a mineral scale the model results predict that materials with high Lu/Hf ratios (blue curves in Figure 7) relative to whole rock (pink curves in Figure 7) will have a neutron-fluence corrected  $^{176}\text{Hf}/^{177}\text{Hf}$  ratio that is too low for its age, initial Hf isotope composition, and Lu/Hf ratio. The model predicts the opposite for Lu/Hf ratios much less than the whole rock (red and light blue curves in Figure 7) where the fluence corrected  $^{176}\text{Hf}/^{177}\text{Hf}$  ratios will be lower than the true isotope composition. These fluence corrections are thus predicted to result in a counterclockwise rotation of the isochron; corrections on the samples in epsilon notation include (12HN20 =  $+ 2.82 \pm 0.5$ , 12HN21 =  $+1.76 \pm 0.5$ , and 12HN22 =  $2.37 \pm 0.5$ ). This result, while possible, would require that the fluence effects be felt on a mineral scale, and the data indicate that this was not the case based on the consistency of Gd and  $^{180}\text{Hf}$  anomalies for the different mineral aliquots. Figure 8 demonstrates this with a plot of mass bias corrected  $\epsilon^{180}\text{Hf}$  against  $^{176}\text{Lu}/^{177}\text{Hf}$  ratio where there is no evidence for this effect for the samples analyzed here within the uncertainty of the measurements. It is important to note, however, that the sensitivity of mass bias corrected  $^{180}\text{Hf}/^{177}\text{Hf}$  to

Lu/Hf ratio is significantly less than that for the  $^{176}\text{Hf}/^{177}\text{Hf}$  ratio (Figure 7) so we cannot completely rule out this effect based on the samples studied here.

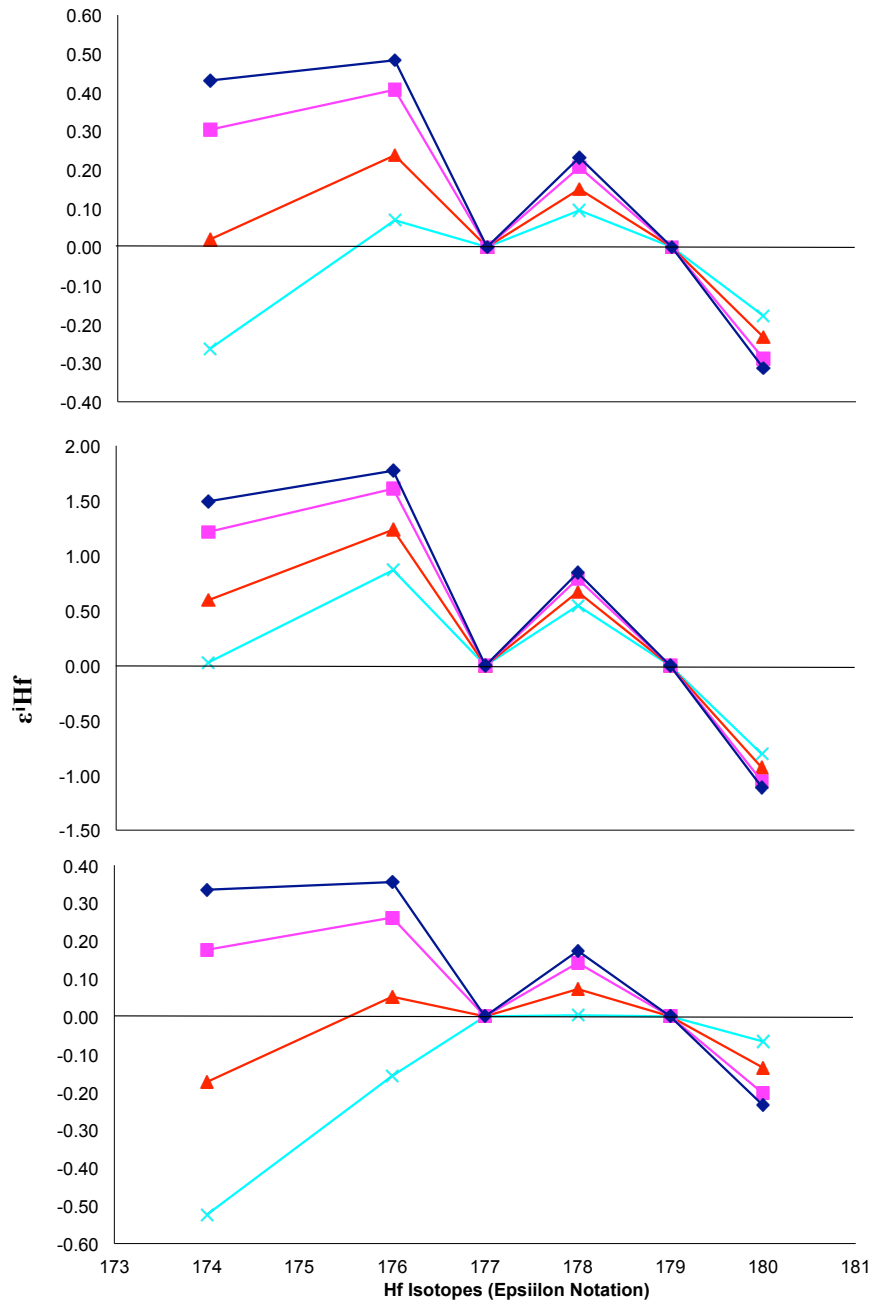


Figure 7. The Hf isotopes on x-axis and  $\epsilon$  units on y-axis. 0.1 of the original Lu/Hf ratio (Dark Blue Diamonds), original Lu/Hf ratio (Pink Squares), 3-times the original Lu/Hf ratio (Yellow Triangles) and 5-times the original Lu/Hf ratio (Light Blue X's). Modeled data showing the variation in  $\epsilon^{\text{Hf}}$  abundances based on variations in the Lu/Hf ratio at three different temperatures: 273.15 K (top) and then the extreme model temps, 20 K (middle) and 520 K (bottom).

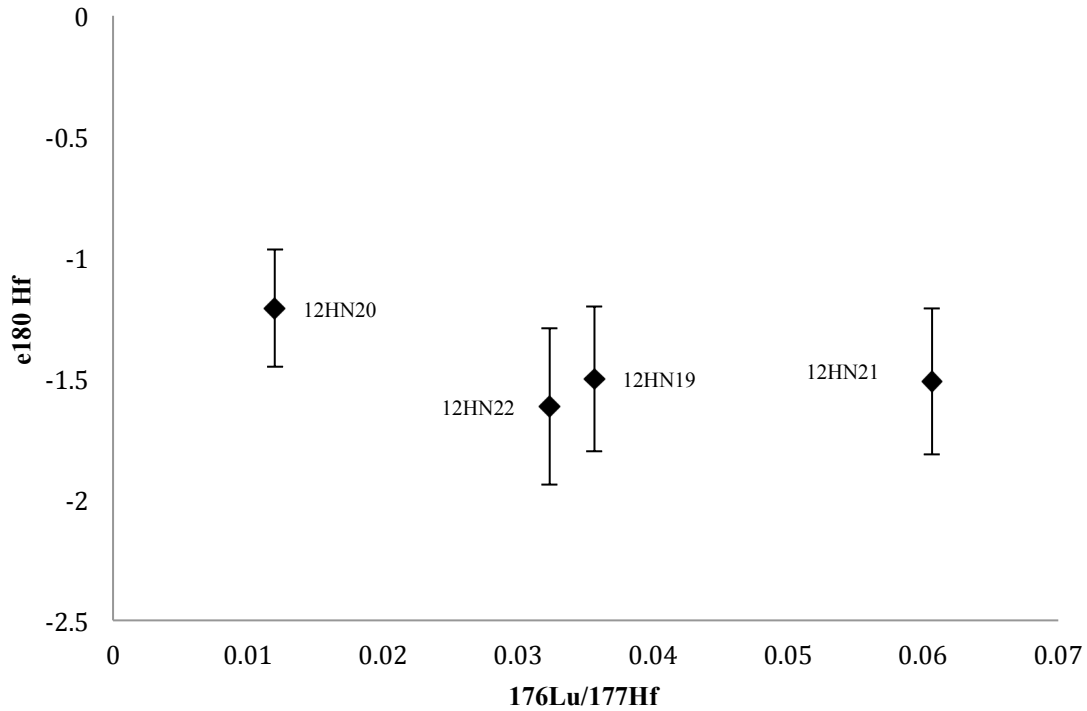


Figure 8. Displays the  $\epsilon^{180}\text{Hf}$  anomaly plotted against the  $^{176}\text{Lu}/^{177}\text{Hf}$  ratio. Shows no correlation between the two values suggesting that there is not a fluence effect felt on a mineral scale, and that the effects are most likely felt on a bulk rock scale. Error bars are set at 10%.

Figure 8 coupled with the Gd and  $^{180}\text{Hf}$  anomaly consistencies seems to confirm that the Lu/Hf ratio variation on a mineral scale had no bearing on the degree of fluence felt by each mineral, which strongly suggests that the fluence effects were felt on a bulk rock scale. The end result was an identical correction applied to each sample, causing no change to the slope of the isochron, and only affecting the initial  $^{176}\text{Hf}/^{177}\text{Hf}$  ratio. The initial  $^{176}\text{Hf}/^{177}\text{Hf}$  value is difficult to constrain quantitatively because I observed that while we use  $^{180}\text{Hf}$  to monitor the fluence effects on the sample the isotope is not as sensitive to changes in temperature while the  $^{176}\text{Hf}$  isotope is much more sensitive

(Figure 7). The result is a bulk scale corrected age of  $4.418 \pm 0.022$  Ga (MSWD = 1.7), Figure 12, which is not different from the uncorrected age.

The Sm-Nd system was corrected using the measured Sm isotopic compositions from sample 78236,28 in place of ‘normal’ Sm values in the data reduction spreadsheet. The substitution of measured Sm values for ‘normal’ Sm values caused the spreadsheet to re-calibrate my samples to the irradiated Sm values thus eliminating the fluence effect for the Sm concentration. For Nd the largest shift from fluence occurs on  $^{143}\text{Nd}$ , which is also the radiogenic daughter. Therefore we would need to look at  $^{145}\text{Nd}$ , except this Nd isotope is difficult to measure accurately and the shift we did measure is less than 0.1 epsilon units. In addition to the aforementioned difficulties the temperature of the 78236,28 system is difficult to constrain precisely and therefore resides somewhere in the commonly accepted lunar surface range of 200 K to 400 K (Lingenfelter et al. 1972, Hidaka et al. 2006). The problem with falling back on this range is that there is a  $0.33\epsilon - 0.44\epsilon$  range in fluence effects depending on the temperature in addition to the existing measurement error. Based on the constant Gd and  $^{180}\text{Hf}$  anomalies that we measured we can assume that the fluence effect is felt on a bulk scale and therefore, similar to Lu-Hf, a correction on the Nd would cause the isochron to retain its slope, but shift the initial  $^{143}\text{Nd}/^{144}\text{Nd}$  value up by 0.33 to 0.44 epsilon units. A review of the fluence pathways and relative sizes can be found in *Appendix II*.

### 4.3 Sm-Nd isotope data

To determine the Sm-Nd isochron for Apollo 17 norite 78236,28 I successfully picked, separated and processed through ion exchange column chromatography four mineral phases and a whole rock aliquot, which yielded a neutron-fluence corrected age of  $4.448 \pm 0.032$  Ga ( $2\sigma$  error ellipses) with a MSWD of 2.3 (Figure 9) and an initial  $^{143}\text{Nd}/^{144}\text{Nd}$  value of  $0.507024 + (0.33\varepsilon - 0.44\varepsilon) \pm 0.000038$  ( $2\sigma$ ). The five separates that were used to determine the age were a hand picked plagioclase sample weighing 52.4 mg, a hand picked pyroxene separate weighing 55.4 mg, a hand picked pyroxene sample with noticeable oxide inclusions weighing 51.43 mg, a hand picked plagioclase sample with noticeable oxide inclusions combined with oxide phases recovered from the thallium malonate chemistry weighing 53.85 mg, and an unpicked whole rock sample weighing 51.57 mg.

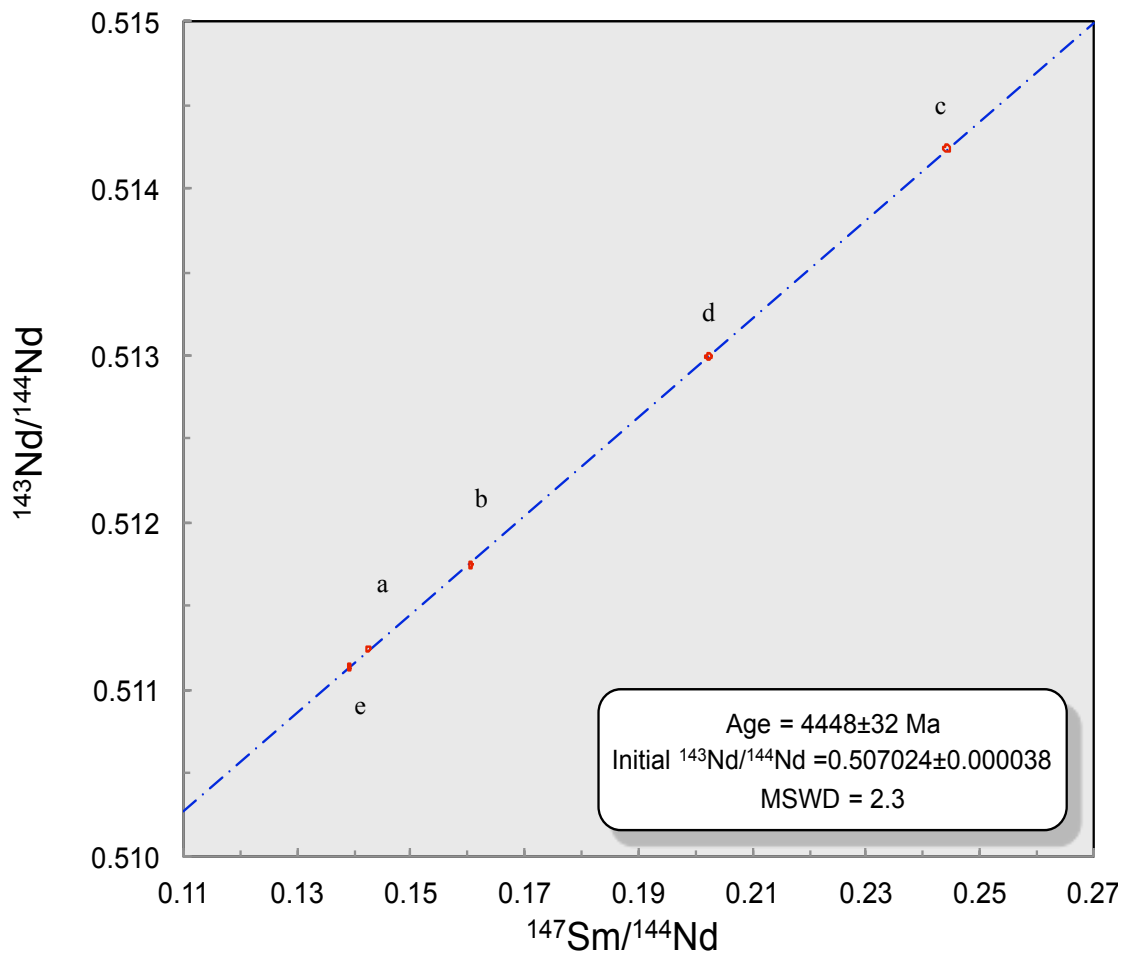


Figure 9. 5- point Sm-Nd isochron representing an age of  $4.448 \pm 0.032$  Ga with an MSWD of 2.3 and an initial  $^{143}\text{Nd}/^{144}\text{Nd}$  value =  $0.507024 + (0.33\epsilon - 0.44 \epsilon) \pm 0.000038$ . Error is represented as error ellipses. Data point letters correspond to data table letters.

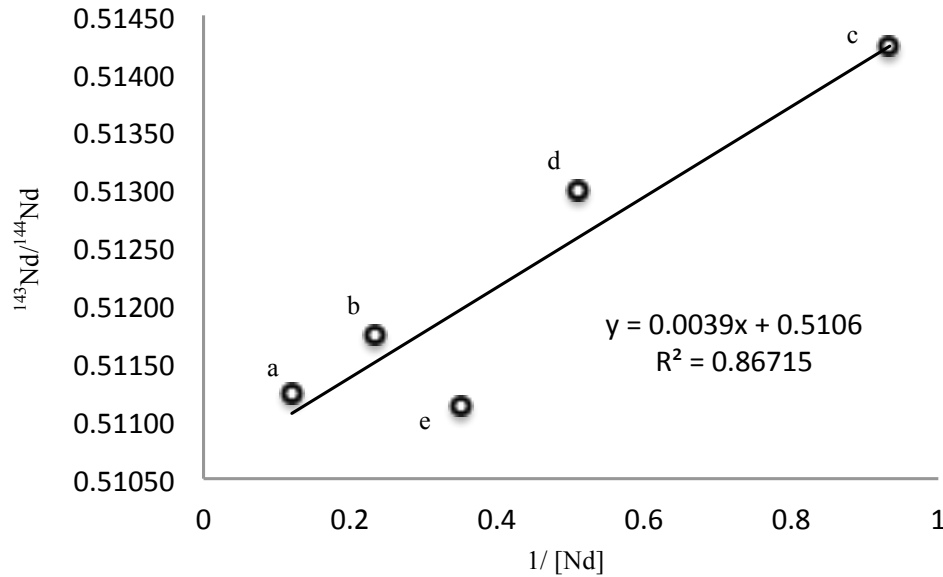


Figure 10. Mixing line using Sm-Nd data. Shows a correlation between points a-c and an outlying point e with an  $R^2 = 0.86715$ . The relationship between the data points could suggest a slight system disturbance for Sm-Nd

Figure 10 shows the samples used in the isochron calculation represented on a  $^{143}\text{Nd}/^{144}\text{Nd}$  vs.  $1/\text{[Nd]}$  plot. This chart shows that there is not likely a 2-component mixing relationship between 4 of the samples with the 5<sup>th</sup> most outlying sample representing the plagioclase + oxide fraction which sits squarely on the isochron in Figure 9, 12HN25. Lapen et al. (2010) showed that the Sm-Nd is especially susceptible to resetting for a number of reasons one of which was the concentration of the daughter product in easily altered phosphate phases. The age yielded by five separates from this study is equal within error to the U-Th-Pb age obtained by Premo and Tatsumoto (1992) and the Sm-Nd age by Nyquist et al. (1981), and the 3-point Lu-Hf age reported in this study, but is ~100 Ma older than more recent ages published by Nyquist et al. (2008) and Edmunson et al. (2009) for samples 78236 and 78238 respectively.

Based on the findings mentioned, it can be assumed that the age,  $4.448 \pm 0.032$  Ga, seems to represent a robust correlation in sample 78236,28.

#### **4.4 Lu-Hf isotope data**

The Lu-Hf system appears to have been disturbed as evidenced by scatter of data points on an isochron diagram. The uncorrected 3-point Lu/Hf isochron yielded an age of  $4.419 \pm 0.023$  Ga, an initial  $^{176}\text{Hf}/^{177}\text{Hf}$  value of  $0.279777 \pm 0.000017$  and  $\text{MSWD} = 1.7$  and the uncorrected 5-point Lu/Hf linear relationship yielded a line with a slope representing an age of  $4.09 \pm 0.72$  Ga, an initial value of  $0.28009 \pm 0.00047$  and  $\text{MSWD} = 820$  (Figure 11). The neutron-fluence corrected Lu-Hf age results in an age that is identical within error to the uncorrected 3-point age, but with a lower, sub-chondritic initial  $^{176}\text{Hf}/^{177}\text{Hf}$  ratio. The neutron-fluence corrected age of  $4.418 \pm 0.022$  Ga ( $2\sigma$  error ellipses)  $\text{MSWD} = 1.7$  (Figure 12) is substantially more accurate and precise than the 5-point isochron, and agrees with our Sm-Nd-fluence corrected age of  $4.448 \pm 0.032$  Ga. The two data points that fall off the line are a whole rock cut and plagioclase + oxide cut. These data points exhibit characteristics of perhaps not being properly equilibrated with the spike during dissolution (Lapen et al. 2004), or those two samples encountered a contaminant at some point in the disaggregation/digestion process, or those fractions have been altered during post-crystallization impact metamorphism. The two former hypotheses are unlikely because all of the sample cuts were handled in an identical manner throughout the various stages from disaggregation to analysis, and if a contaminant were present it would be

expected to affect all samples in a similar manner, which was not observed. In addition to the age of  $4.418 \pm 0.022$  Ga ( $2\sigma$  error ellipses) MSWD = 1.7 (Figure 12), we modeled the age assuming a mineral scale fluence effect on 78236,28. The mineral scale fluence correction resulted in an age of  $4.446 \pm 0.023$  Ga ( $2\sigma$  error ellipses) MSWD = 1.8 (Figure 13), and the  $^{176}\text{Hf}/^{177}\text{Hf}$  shifts for the bulk correction vs. the mineral scale correction are in table 7. While this age better agrees with the Sm-Nd age of  $4.448 \pm 0.032$  Ga, the initial daughter ratio is significantly lower than when a bulk scale correction is applied. This further decrease in initial value coupled with consistent Gd and  $^{180}\text{Hf}$  anomalies from the measured data tend to suggest that a mineral scale correction is not ideal, but cannot be ruled out.

	Bulk Correction $^{176}\text{Hf}/^{177}\text{Hf} \pm 2\text{SE}$	Mineral Correction $^{176}\text{Hf}/^{177}\text{Hf} \pm 2\text{SE}$
12HN20	$0.280741 \pm 17$	$0.280733 \pm 17$
12HN21	$0.284921 \pm 14$	$0.284941 \pm 14$
12HN22	$0.282474 \pm 18$	$0.282478 \pm 18$

Table 7. Table shows bulk correction shifts on  $^{176}\text{Hf}$  vs. mineral scale correction shifts. Errors listed are measured errors, but also include an additional  $\pm 0.5$  epsilon unit uncertainty from error propagated during the modeling.

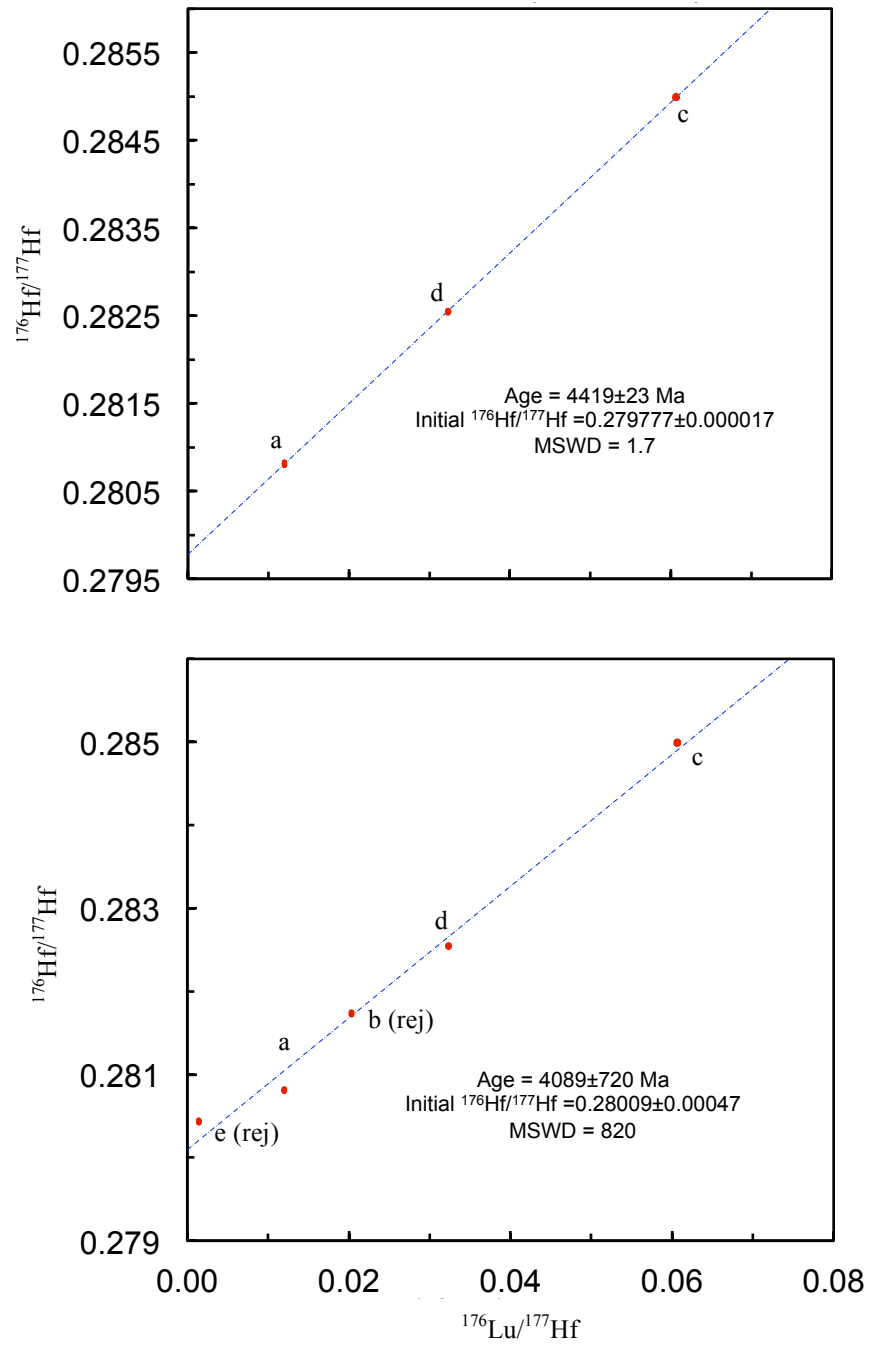


Figure 11. A) Uncorrected neutron-fluence affected Lu/Hf 3-point isochron of age  $4.419 \pm 0.023$  Ga, MSWD = 1.7. B) Uncorrected neutron-fluence affected Lu/Hf 5-point isochron of age  $4.089 \pm 0.720$  Ga, MSWD = 820. Both A & B have  $^{176}\text{Hf}/^{177}\text{Hf}$  initials that are less than the solar system, which is a product of the neutron-fluence effect. Error is represented as error ellipses.

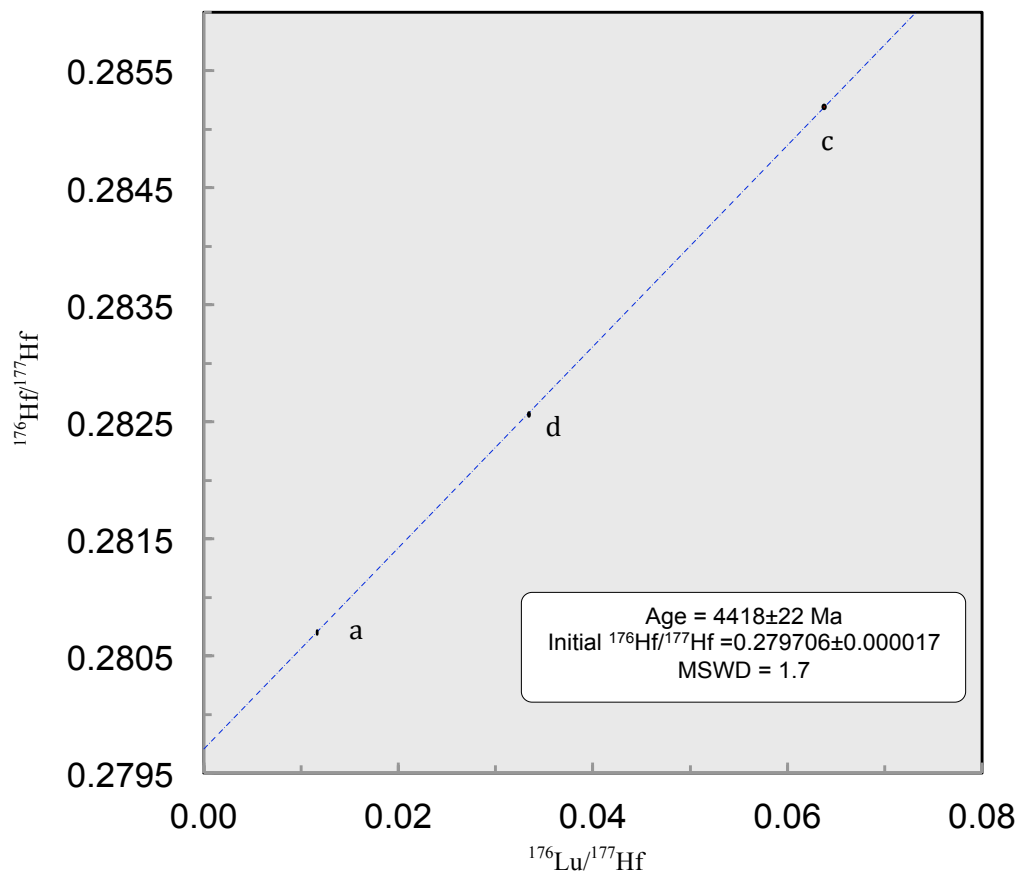


Figure 12. Lu-Hf isochron from 78236,28 samples 12HN20 (a), 12HN21 (c) and 12HN22 (d). The low  $^{176}\text{Hf}/^{177}\text{Hf}$  ratio is concerning because it is ‘impossibly’ lower than CHUR and sub-BABI values, defined in this paper as the Basaltic Achondrite Best Initial based on Bizzarro et al. (2012). Error ellipses ( $2\sigma$ ).

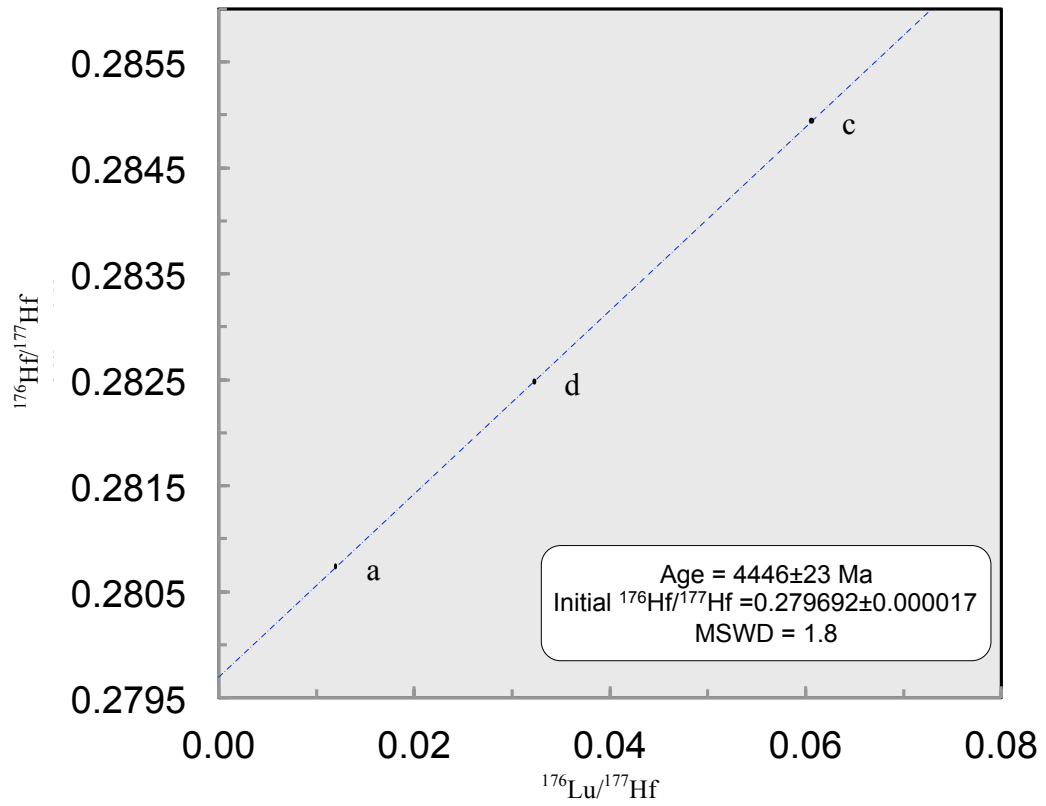


Figure 13. Lu-Hf isochron from 78236,28 samples 12HN20 (a), 12HN21 (c) and 12HN22 (d). The low  $^{176}\text{Hf}/^{177}\text{Hf}$  ratio coupled with the much older age result in an isochron with a near sub-solar system initial based on the Bizzarro et al. 2012 achondrite derived initial of 0.279685.

## Chapter 5

### Discussion

#### 5.1 Modeled neutron fluence effects on Lu-Hf

As demonstrated earlier in sections 3.5 and 4.2, the modeled Hf isotope data matches well with measured data for 78236,28, with the exception that measured  $^{180}\text{Hf}$  and  $^{178}\text{Hf}$  values were more elevated than the model. The elevated model pattern from my measured data appears to be the result of a greater sensitivity of Hf to neutron fluence effects than predicted by the model, which could be related to the effective capture cross section concept (Lingenfelter et al. 1972). The concept demonstrated in Lingenfelter et al. (1972), shows that in samples with elevated levels of major element neutron absorbers such as Fe and Ti, there is a notable decrease in the capture effectiveness of other trace element neutron absorbers like Sm and Gd due to overlap in the absorption frequencies. Epsilon  $^{180}\text{Hf}$  anomalies measured in the unspiked sample aliquot from 78236,28 are  $\sim 1.0$  epsilon unit larger than values calculated in the model, which used  $^{149}\text{Sm}$  as a neutron flux monitor. These  $^{180}\text{Hf}$  anomalies are real anomalies produced by the mass bias correction, and can be used as an indicator of fluence effects on the Hf system. Since the model utilized the  $^{149}\text{Sm}$  isotope shift to calculate the  $\Psi$  values used in estimating the fluence effects on the system,  $^{149}\text{Sm}$  is an inadequate isotope to use to correct the Lu-Hf system at least in the case of sample 78236,28. The  $^{180}\text{Hf}$  anomalies based on the neutron capture shift of  $^{157}\text{Gd}$  should be  $\sim 6x$  larger than those of  $^{149}\text{Sm}$  due to the much larger

capture cross section size of 239,000 barns, but we observed, in the modeled data, that using  $^{157}\text{Gd}$  produced  $^{180}\text{Hf}$  anomalies that were  $\sim 1.6x$  larger than Sm. The lack of sensitivity observed confirmed that Gd would also be an inadequate element to use when correcting for neutron flux effects in the Lu-Hf system for sample 78236,28. Because the sensitivity of Hf to the neutron-fluence effects was much greater than what was predicted using  $^{149}\text{Sm}$ , it can be assumed that Sm and Gd have much smaller effective capture cross section than the model assumed. One potential cause for these effects seen is defined in Lingenfelter (1972) where the effective capture cross-section concept was established. The concept accounts for all major neutron absorbers in the system to calculate a representative capture cross section,  $\Sigma_{\text{eff}}$ . If these major neutron absorbers were interfering with Sm and Gd in the 78236,28 system by depleting the neutron budget then  $^{149}\text{Sm}$  and  $^{157}\text{Gd}$  would be underestimating the neutron flux, which is consistent with our model predictions. Further work is being conducted to look into the absorption frequencies of the various neutron absorbers in the system, but detailed investigation of the issue is beyond the scope of this thesis. Since an elevated sensitivity in the Hf isotopes is observed in the model, it can be suggested that the Hf absorption frequency does not overlap with some of the other major neutron absorbers in 78236,28, and while it is known that Hf can absorb multiple neutrons at once causing the effectiveness of the capture cross-section to be amplified (Schemel, 1977 and references therein) it is likely not happening here based on the patterns observed in the model. This would allow for Hf to preferentially absorb more of the free neutrons in the budget. These observations suggest that unspiked Hf would be a superior neutron fluence monitor to use for neutron flux corrections in the Lu-Hf system more so than the conventional  $^{149}\text{Sm}$  method used

by other authors, and used by Edmunson et al. (2009) on Sm-Nd systematics with Apollo 17 sample 78238. We also attempted to test the robustness of our model by varying the Hf abundance starting compositions from CHUR. We varied the values in accordance with the  $^{176}\text{Hf}/^{177}\text{Hf}$  variation we observed in the mineral separates. The model output the same epsilon values we varied, telling us that the Hf starting values would not affect the reliability of the model. We then investigated the effect of the  $^{176}\text{Lu}/^{177}\text{Hf}$  composition might have on the model. As seen in chapter four by varying the  $^{176}\text{Lu}/^{177}\text{Hf}$  ratio we observed in the model that if neutron fluence was affecting the sample on a mineral scale, we would see a counterclockwise rotation of the isochron after correction. In addition a variation in the  $^{180}\text{Hf}$  anomaly and Gd anomaly values would change based on mineral composition, but again we do not observe this in the measured Hf and Gd isotope data. From the measurements and modeling, four major conclusions can be drawn; first, the conventional correction methods are not adequate enough to correct for the fluence effects observed in sample 78236,28, Second, further investigation is needed to determine the reasons for  $^{149}\text{Sm}$  and  $^{157}\text{Gd}$  not adequately being able to correct the fluence effects in 78236,28, third the fluence effects felt by the sample are felt on a bulk scale rather than a mineral scale, and fourth the fluence correction on the Lu/Hf system in 78236,28 is temperature independent and is most likely temperature independent for other samples of similar compositions.

## 5.2 Chronology of 78236

The Sm-Nd isotope systematics of sample 78236,28 produce an age of  $4.448 \pm 0.032$  Ga, and initial  $^{143}\text{Nd}/^{144}\text{Nd}$  value of  $0.507024 + (0.33\varepsilon - 0.44\varepsilon) \pm 0.000038$  ( $2\sigma$ ) and an MSWD = 2.3. The Sm-Nd mixing line plot does indicate a slight correlation possibly suggesting a system disturbance, which could be corroborated by the  $\sim 100$  Ma older age. Otherwise the Sm-Nd age of 78236,28 seems robust with an MSWD = 2.3 and a correlation between 5 different aliquots, and the fact that we see an agreement, within error, to our neutron-fluence corrected Lu-Hf age of  $4.418 \pm 0.022$  Ga.

The Lu-Hf isotope systematics of sample 78236,28 shows signs of being disturbed. Among the 5 samples analyzed, 3 formed a very good isochron with a slope representing a bulk scale neutron-fluence corrected age of  $4.418 \pm 0.022$  Ga, an initial  $^{176}\text{Hf}/^{177}\text{Hf}$  value of  $0.279706 \pm 0.000017$  and an MSWD = 1.7, and a mineral scale fluence corrected age of  $4.446 \pm 0.023$  Ga ( $2\sigma$  error ellipses) an initial  $^{176}\text{Hf}/^{177}\text{Hf}$  value of  $0.279692 \pm 0.000017$  MSWD = 1.8 (Figure 13), with two of the data points falling far off the line perhaps related to shock disturbance, or less likely, spike-sample equilibration issues. While both of the interpreted ages of the 3-point Lu-Hf isochrons represent ages that are in agreement with previous studies shown in table 8, the initial  $^{176}\text{Hf}/^{177}\text{Hf}$  value is problematic in both instances, but more so in the mineral scale neutron-fluence corrected age. We do not see the same disturbances in the Sm-Nd systematics, suggesting that there is something preferentially decoupling the Lu-Hf systematics.

	Pb/Pb	U/Pb	Rb/Sr	Sm/Nd	Lu/Hf	Ar/Ar
Hinthorne 1977 (78235)	4.25 ± 0.09 Ga					
Premo & Tatsumoto 1992 (78235/78236)		4.426 ± 0.065 Ga				
Nyquist 1981 (78236)			4.38 ± 0.02 Ga	4.43 ± 0.05 Ga		4.39 Ga
Carlson & Lugamir 1982 (78236)				4.34 ± 0.04 Ga		
Aeschlimann 1982 (78235)						4.11 ± 0.02 Ga
Edmunson 2009 (78238)	4.333 ± 0.059 Ga		4.366 ± 0.053 Ga	4.334 ± 0.037 Ga		
This Study (78236,28)				4.448 ± 0.032 Ga	4.446 ± 0.023 Ga	

Table 8. Published ages for Apollo 17 samples 78235/78236/78238. C. Meyer, Lunar Sample Compendium.

The bulk scale fluence corrected initial  $^{176}\text{Hf}/^{177}\text{Hf}$  value represents a value that is  $\sim 0.2$  epsilon units greater than the initial of the solar system (Figure 13; Bizzarro et al., 2012) based on what is referred to here as the Bizzarro's basaltic achondrite best initial (B-BABI). The bulk scale corrected initial  $^{176}\text{Hf}/^{177}\text{Hf}$  is 'impossibly' less than the initial solar system value of CHUR (Figure 14; Bouvier et al. 2008). These data may indicate that the Lu-Hf isotope system is more susceptible to disturbance in this lunar lithology, that the neutron fluence corrections are inaccurate, or that the moon began with an initial  $^{176}\text{Hf}/^{177}\text{Hf}$  ratio that is similar to that determined by Bizzarro et al. (2012) and Thrane et al. (2010). Given the modeling of the neutron effects on the Lu-Hf isotope system that indicate positive anomalies in the  $^{176}\text{Hf}/^{177}\text{Hf}$  ratio (i.e. a correction that would lower the ratio), it is unlikely that the corrections could account for a very low  $^{176}\text{Hf}/^{177}\text{Hf}$  ratio relative to CHUR or B-BABI. The previous statement leaves metamorphic disturbance or differences in initial  $^{176}\text{Hf}/^{177}\text{Hf}$  between chondrites and the Moon. Since the Sm-Nd isotope system can be more easily disturbed than the Lu-Hf isotope system in some rocks (e.g. Shafer et al., 2010; Lapen et al., 2010) it seems unlikely that the sample was greatly disturbed given the tight, low-scatter nature of the Sm-Nd isochron (Figure 6), but this is

only speculative. Testing the hypothesis that there are variations in initial  $^{176}\text{Hf}/^{177}\text{Hf}$  ratios in solar system materials is beyond the scope of this study.

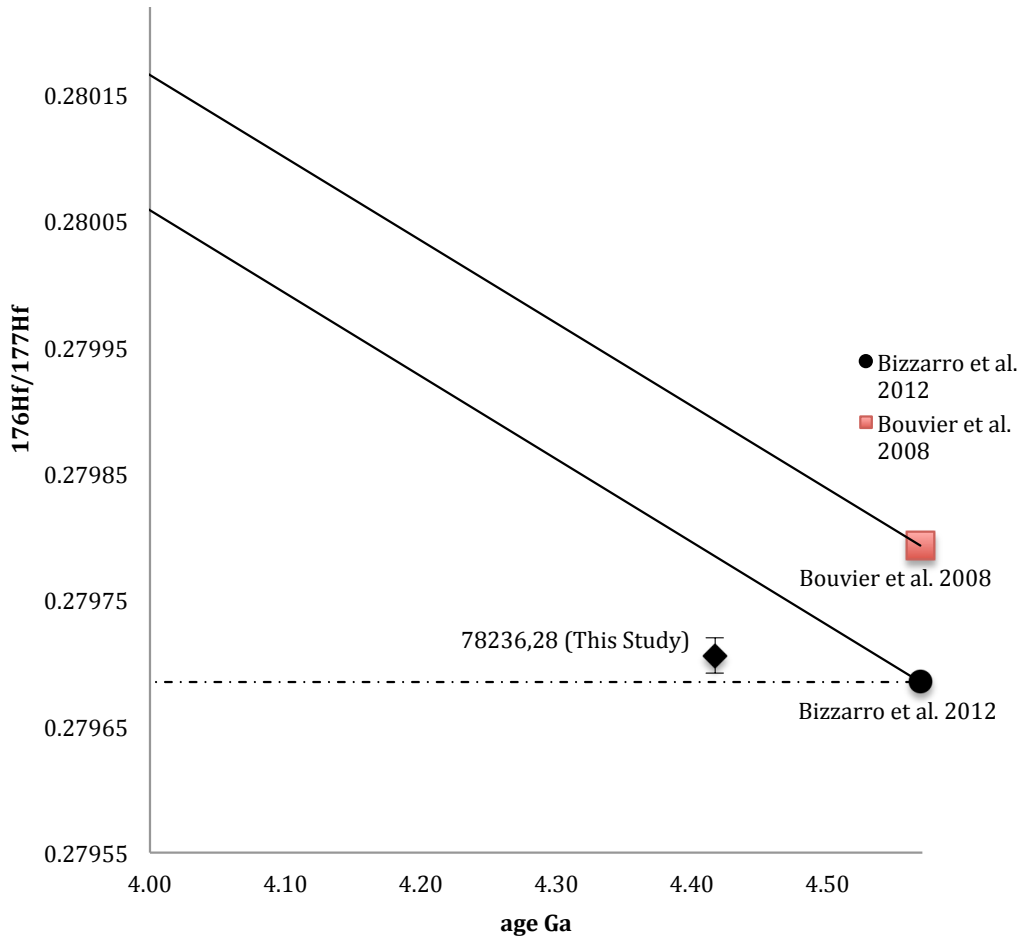


Figure 14. Figure shows relation of measured  $^{176}\text{Hf}/^{177}\text{Hf}$  of sample 78236,28 to CHUR and B-BABI evolutionary lines published by Bouvier et al. 2008 and Bizzarro et al. 2012 respectively. All data are normalized to the JMC 475 standard value published by Vervoort and Blichert-Toft 1999. Error on 78236,28 is  $\pm 0.005\%$ , based on error calculated from  $^{180}\text{Hf}$  and  $^{178}\text{Hf}$  anomalies during the fluence modeling.

## Chapter 6

### Conclusions

Based on the observations made between the measured Lu-Hf data of Apollo 17 sample 78236,28 specifically the  $^{178}\text{Hf}$  and  $^{180}\text{Hf}$  anomalies, it is clear that the sample displayed effects of irradiation through neutron bombardment. After modeling the effects of neutron flux on the Lu-Hf system using model data from the Brookhaven National Nuclear Database, it is obvious that the patterns observed in the model data match the patterns observed in the measured data of sample 78236,28, further implicating thermal neutron fluence as the culprit behind the Hf anomalies. The thermal neutron fluence model utilized the  $^{149}\text{Sm}$  isotope as a gauge for the degree of thermal neutron fluence experienced by the Hf system, similar to methods used by Nyquist (1995), Hidaka et al. (2000, 2006, 2012), Brandon et al. (2009), and Edmunson et al. (2009). The observed effects were  $^{149}\text{Sm}$  did not produce a large enough correction for the effects on the Hf system suggesting that other elements (likely Fe and Ti) are competing with Sm and Gd for the free neutron budget. Modeling effectiveness was based on the modeled  $^{180}\text{Hf}$  anomaly compared to what was actually measured in the unspiked 78236,28 sample. We observe the model producing  $^{180}\text{Hf}$  anomalies that were far too small to represent what was measured in the unspiked sample. However, in the model, we did observe signs of increased sensitivity from Hf to neutron fluence beyond what we had predicted based on capture cross section size. The elevated sensitivity of our model suggests that Hf has a

larger effective capture cross section than predicted by the model. Since  $^{177}\text{Hf}$  is the normalizing isotope in the Lu-Hf system, analysis would require an unspiked WR as well as spiked samples in order to properly correct the neutron flux effects. In addition to the modeling, the Sm-Nd isotope systematics produced an age  $4.448 \pm 0.032$  Ga with an MSWD of 2.3, which is in agreement with earlier published ages for the sample as well as the Lu-Hf measurements presented in this study of  $4.446 \pm 0.23$  Ga (mineral scale correction age), and  $4.418 \pm 0.022$  Ga (bulk scale correction age). The Sm-Nd age, however, is  $\sim 100$  Ma older than recently published works from Edmunson et al. (2009) and Nyquist et al. (2008) on samples 78238 and 78236 respectively. The age and extremely low initial radiogenic ratio for the Lu-Hf system tends to suggest a system disturbance of some sort, although the 3-point isochrons presented in this thesis have an ideal correlation. Further work is currently being conducted to improve the robustness of the 3-point isochron by adding one to two more data points. The fluence correction on the Lu-Hf system in lunar samples is important for a proper understanding of the evolution of the Earth-Moon system, and although the corrections made in this thesis are minor other lunar samples might have been exposed longer or will have larger Lu/Hf ratios where the effect will be amplified.

Further investigations need to be conducted for the thermal neutron fluence effects on lunar samples, specifically the Lu-Hf system, as well as an investigation into the absorption frequencies of various isotopes contained in these samples.

## References

- Albarede, F., Scherer, E.E., Blichert-Toft, J., Rosing, M., Simionovici, A., and Bizzarro, M. (2006), Gamma-ray irradiation in the early solar system and the conundrum of the  $^{176}\text{Lu}$  decay constant. *Geochimica et Cosmochimica Acta*. **70**:1261-1270.
- Andreasen, R., and Sharma, M. (2006), Solar nebula heterogeneity in p-process Samarium and Neodymium isotopes. *Nature*. **314**:806-809.
- Bizzarro, M., Connelly, N., Thrane, K. and Borg, L. E. (2012), Excess Hf-176 in meteorites and the early Earth zircon record. *Geochem. Geophys. Geosyst.*, **13**, Num. 3
- Blanchard, D.P. (1982), The Chemistry of Pristine Lunar Samples. Magmatic Processes of Early Planetary Crusts: Magma Oceans and Stratiform Layered Intrusions: *Lunar and Planetary Institute Workshop*. p.(49).
- Blichert-Toft, J. (2001), On the Lu-Hf isotope geochemistry of silicate rocks. *Geostand. Newsl.*, **25**(1), 41-56.
- Borg, L.E., Connelly J. N., Boyet M., and Carlson, R. W. (2011), Chronological evidence that the Moon is either young or did not have a global magma ocean. *Nature*. **477**:70-72.
- Borg, L.E., Norman, M.D., Nyquist, L., Bogard, D., Snyder, G., Taylor, L. Lindstrom, M. (1999), Isotopic studies of ferroan anorthosite 62236: A young lunar crustal rock from a light REE depleted source. *Geochimica et Cosmochimica Acta*. **63**:2679-2691.
- Borg, L.E., Norman, M.D., Nyquist, Taylor, L., Wiessmann, H., Shih, C-Y. (1997a), Constraints on Martian differentiation processes from Rb-Sr and Sm-Nd isotopic analyses of the basaltic shergottite QUE 94201. *Geochimica et Cosmochimica Acta*. **61**:4915-4931.
- Bouvier, A., Vervoort, J.D., and Patchett, P.J. (2008), The Lu-Hf and Sm-Nd isotopic compositions of CHUR: Constraints from unequilibrated chondrites and implications for the bulk composition of terrestrial planets. *EPSL*. **273**:48 – 57.
- Boyet, M. and Carlson, R.W. (2007), A highly depleted Moon or a non-magma ocean origin for the lunar crust? *EPSL*. **262**:505-516.
- Brandon, A.D., Lapen, T.J., Debaille, V., Beard, B.L., Rankenburg, K., and Neal, C. (2009), Re-evaluating  $^{142}\text{Nd}/^{144}\text{Nd}$  in lunar mare basalts with implications for the early evolution and bulk Sm/Nd of the Moon. *Geochimica et Cosmochimica Acta*. **73-20**:6421-6445.

Carlson R.W. and Lugmair G.W. (1981a), Time and duration of lunar highlands crust formation. *EPSL*. **52**:227- 238.

Dymek, R.F., Albee, A.L. and Chodos, A.A. (1975b), Comparative petrology of lunar cumulate rocks of possible primary origin: Dunite 72415, troctolite 76535, norite 78235, and anorthosite 62237. *Proc. 6th Lunar Sci. Conf.* 301-341.

Edmunson, J., Borg, L.E., Nyquist, L.E. and Asmerom, Y. (2009) A combined Sm–Nd, Rb–Sr, and U–Pb isotopic study of Mg-suite norite 78238: Further evidence for early differentiation of the Moon. *Geochimica et Cosmochimica Acta*. **73**:514-527.

Elardo, S.M., Draper, D.S., and Shearer, C.K. (2011), Lunar magma ocean crystallization revisited: Bulk composition, early cumulate mineralogy, and the source regions of the highlands Mg-suite. *Geochimica et Cosmochimica Acta*. **75-11**:3024-3045.

Eugster, O., Tera, F., Burnett, D. S., & Wasserburg, G. J. (1970), Isotopic composition of Gadolinium and neutron capture effects in some meteorites. *J. Geophys. Res.*, **75**, 2753.

Gao, Y., Huang, J., and Casey, J.F. (2009), Data report: trace element geochemistry of oceanic crust formed at superfast-spreading ridge, Hole 1256D. *Proceedings of the Integrated Ocean Drilling Program*. Vol. **309/312**.

Hidaka, H., Ebihara, M., Yoneda, S. (2000), Neutron capture effects on samarium, europium, and gadolinium in Apollo 15 deep drill-core samples. *Meteorit. Planet. Sci.* **35**:581–589.

Hidaka, H., Yoneda, S., and Marti, K. (2006), Regolith history of the aubritic meteorite parent body revealed by neutron capture effects on Sm and Gd isotopes. *Geochimica et Cosmochimica Acta*. **70-13**:3449-3456.

Hidaka, H., Kondo, T., and Yoneda, S. (2012), Heterogeneous isotopic anomalies of Sm and Gd in the Norton county meteorite: Evidence for irradiation from the active early Sun. *The Astrophysical Journal*. **746:132** (8pp).

Hiesinger, H. and Head, J.W. (2006), New Views of Lunar Geoscience: An Introduction and Overview. *Reviews in Mineralogy and Geochem.* **60**:1-81.

Hinthorne, J.R., Conrad, R.L. and Church, S.E. (1977), Lead lead age and rare earth element determinations in lunar norite 78235 (abs). *Lunar Sci.* **VIII**:444-446. Lunar Planetary Institute, Houston.

Jackson, E.D., Sutton, R.L. and Wilshire, H.G. (1975), Structure and petrology of a cumulus norite boulder sampled by Apollo 17 in Taurus-Littrow valley, the Moon. *Geol. Soc. Am. Bull.* **86**:433-442.

Lapen, T.J., Mahlen, N.J., Johnson, C.M., Beard, B.L. (2004), High precision Lu and Hf isotope analyses of both spiked and unspiked samples: A new approach. *Geochem. Geophys. Geosyst.*, **5**, Q01010, doi: 10.1029/2003GC000582.

Lapen, T.J., Richter, M., Brandon, A.D., Debaille, V., Beard, B.L., Shafer, J.T., Peslier, A.H. (2010), A Younger Age for ALH84001 and Its Geochemical Link to Shergottite Sources in Mars. *Science*. **328**:347-349.

Elkins-Tanton, L.T., Burgess, S., and Yin, Q-Z. (2011), The lunar magma ocean: Reconciling the solidification process with lunar petrology and geochronology. *EPSL*. **304**:326-336.

Lingenfelter, R.E., Canfield, E.H., Hampel, V.E. (1972), The lunar neutron flux revisited, *EPSL*. **16**:355–369

Meyer, C. (2010), Lunar Compendium samples: 78236, 67215, 60025 and 15415.

Munker, C., S. Weyer, E. Scherer, and Mezger, K. (2001), Separation of high field strength elements (Nb, Ta, Zr, Hf) and Lu from rock samples for MC-ICPMS measurements. *Geochem. Geophys. Geosyst.* *2*(12), **1064**, doi:10.1029/2001GC000183.

Norman, M. D., Borg, L. E., Nyquist, L. E. and Bogard, D. D. (2003), Chronology, geochemistry, and petrology of a ferroan noritic anorthosite clast from Descartes breccia 67215: Clues to the age, origin, structure, and impact history of the lunar crust. *Meteorit. Planet. Sci.* **38**:645–661.

Nyquist, L. E., Shih, C-Y., and Reese, Y. D. (2008), Sm-Nd For norite 78236 and eucrite Y980318/433: Implications for planetary and solar system processes. *NASA publication*.

Nyquist, L.E. and Shih, C.-Y. (1992), The isotopic record of lunar volcanism. *Geochimica et Cosmochimica Acta*. **56**:2213-2234.

Nyquist, L.E., Wiesmann, H., Bansal, B., Shih, C-Y., Keith J.E., and Harper, C.L. (1995),  $^{146}\text{Sm}$ -  $^{142}\text{Nd}$  formation interval for the lunar mantle. *Geochimica et Cosmochimica Acta*. **59-13**:2817-2837.

Nyquist, L.E., Reimold, W.U., Bogard, D.D., Wooden, J.L., Bansal, B.M., Wiesmann, H. and Shih, C.-Y. (1981b), A comparative Rb-Sr, Sm-Nd and K-Ar study of shocked norite 78236: Evidence of slow cooling in the lunar crust? *Proc. 12th Lunar Planet. Sci. Conf.* 67-97.

Parrington, John R. Nuclides and Isotopes, 15<sup>th</sup> Ed. San Jose: GE Nuclear Energy, 1999.

- Premo, W.R. (1991), Rb-Sr and Sm-Nd ages for lunar norite 78235/78236: Implications on the U-Pb isotopic systematics in this high-Mg rock (abs). *Lunar Planet. Sci.* **XXII**, 1089-1090. Lunar Planetary Institute, Houston.
- Prinzhofer, A.A., Papanastassiou, D.A., and Wasserburg, G.J. (1992), Samarium-Neodimium evolution of meteorites. *Geochimica et Cosmochimica Acta.* **56**:797-815.
- Schemel, J. H. (1977), ASTM Manual on Zirconium and Hafnium. ASTM International. pp. 1-5. ISBN 978-0-8031-0505-8.
- Sclar, C.B. and Bauer, J.F. (1975a), Shock-induced subsolidus reduction-decomposition of orthopyroxene and shock induced melting of norite 78235. *Proc. 6th Lunar Sci. Conf.* 799-820.
- Shearer, C.K. and Papike, J.J. (2005), Early crustal building processes on the moon: Models for the petrogenesis of the magnesian suite. *Geochimica et Cosmochimica Acta.* **69-13**:3445-3461.
- Shearer, C.K., Hess, P.C., Wieczorek, M.A., Pritchard, M.E., Parmentier, E.M., Borg, L.E., Longhi, J., Elkins-Tanton, L.T., Neal, C.R., Antonenko, I., Canup, R.M., Halliday, A.N., Grove, L.G., Hager, B.H., Lee, D.-C., Wiechert, Uwe. (2006), Thermal and magmatic evolution of the Moon. *Reviews in Mineralogy and Geochem.* **60**:365-518.
- Shih, C.-Y., Nyquist, L.E., Dash, E.J., Bogard, D.D., Bansal, B.M. and Wiesmann, H. (1993), Ages of pristine noritic clasts from lunar breccias 15445 and 15455. *Geochimica et Cosmochimica Acta.* **57**:915-931.
- Sprung, P., Scherer, E. E., Upadhyay, D., Leya, I. and Mezger, K. (2010), Non-nucleosynthetic heterogeneity in non-radiogenic stable Hf isotopes: Implications for early solar system chronology. *EPSL*, **295**:1-11.
- Thrane, K., Connelly, J. N., Bizzarro, M., Meyer, B. S. and The, L.-S. (2010), Origin of excess <sup>176</sup>Hf in Meteorites. *The Astrophysical Journal*, **717**:861-867, doi: 10.1088/0004-637X/717/2/861.
- Van Achtenbergh, E., Ryan, C. G. and Griffin, W. L. (1999), GLITTER: On-line interactive data reduction for the laser ablation ICP-MS Microprobe. 9<sup>th</sup> *V. M. Goldschmidt conf.*, 7215 (72pp).
- Vervoort, J.D., Patchett, J.P., Soderlund U. & Baker, M. (2004), Isotopic composition of Yb and the determination of Lu concentrations and Lu/Hf ratios by isotope dilution using MC-ICPMS. *Geochem. Geophys. Geosyst.*, **5**, Num 11 (15pp).

Yamaguchi, A., Taylor, G.J., Keil, K., Floss, C., Crozaz, G., Nyquist, L.E., Bogard, D.D., Garrison D.H., Reese, Y.D., Wiesmann, H., Shih, C-Y. (2001), Post-crystallization reheating and partial melting of eucrite EET 90020 by impact into the hot crust of asteroid 4 Vesta ~4.5 GYr. Ago. *Geochimica et Cosmochimica Acta*. **65**:3577-3599.

## Appendix I: Neutron flux correction model

CD with Excel files available upon request – [stsimmons@uh.edu](mailto:stsimmons@uh.edu), [sammsim87@gmail.com](mailto:sammsim87@gmail.com)

(1) The model utilizes Hidaka et al. equation for calculating fluence:

$$\Psi = -1.0 \times 10^{-4} \epsilon_{149\text{Sm}} / \sigma_{149} \quad (1)$$

(2) Once degree of fluence is determined from equation (1) the model uses the ‘normal’ isotopic abundances multiplied by the elemental abundances, determined from ICP-MS analysis, to calculate isotopic abundances in the sample.

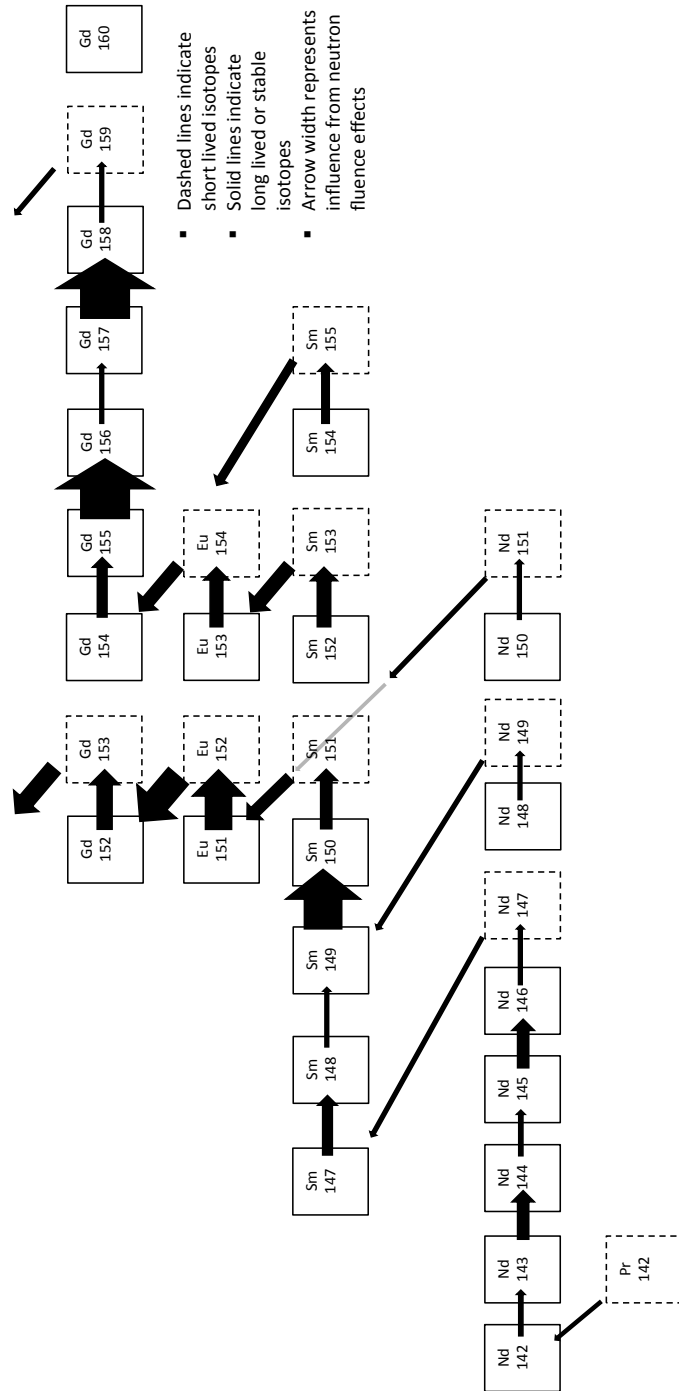
(3) On a separate spreadsheet designed by Rasmus Andreasen the capture cross sections for each isotope were calculated at temperatures varying from 20K to 520K. These cross sections were quality controlled using the Nuclides and Isotopes 15<sup>th</sup> ed. GE Nuclear energy manual.

(4) The calculated cross sections and their respective isotopic abundances were multiplied together along with the degree of fluence to determine amount of fluence felt per isotope.

(5) The combined fluence effects for each isotope were combined and subtracted or added, depending on how the fluence effect was affecting a particular isotope (i.e. effect on <sup>175</sup>Lu was determined by adding the input from <sup>174</sup>Hf and <sup>174</sup>Yb and subtracting the output from <sup>175</sup>Lu as determined by the NF flow chart, Figure 6), from the isotopic abundances to produce a value that represented the amount of fluence per isotope.

(6) A mass bias correction to the data was necessary to carry the data through the same process it would normally go through if being analyzed on the mass spectrometer. The mass bias correction was carried out in an identical manner to the methods described in Lapen et al. (2004) and in Chapter 3 of this thesis.

# Appendix II: Sm-Nd neutron flow model



Neutron flux flow paths in the Sm-Nd system. Arrows scale to the size of the contribution based on a histogram that scaled thermal neutron capture cross section to width.